

Bachelor's Thesis

Implementierung der Jet-Ladung für die dileptonische $t\bar{t}$ Rekonstruktion

Implementation of jet charge for the dileptonic $t\bar{t}$ reconstruction

prepared by

Tobias Fitschen

from Zeven

at the II. Institut of Physics

Thesis number: II.Physik-UniGö-BSc-2015/11

Thesis period: 13th April 2015 until 20th July 2015

First referee: Prof. Dr. Arnulf Quadt

Second referee: Prof. Dr. Ariane Frey

Abstract

Aufgrund des vergleichsweise guten Auflösungsvermögens von Leptonen in Teilchendetektoren ist der dileptonische $t\bar{t}$ Zerfall ein vielversprechender Prozess, um mehr über die fundamentalen Eigenschaften des Top Quarks zu erfahren. Die kinematische Rekonstruktion dieses Zerfallsmodus wird jedoch durch die beiden Neutrinos in dessen Zerfallsprodukten erschwert, da diese in solchen Detektoren nicht direkt nachgewiesen werden können. Dementsprechend wichtig ist es, so viel der zur Verfügung stehenden Information über die beteiligten Teilchen zu nutzen wie möglich. In dieser Arbeit wird die elektromagnetische Ladung der beiden Jets im Endzustand des Prozesses in Relation zu den Ladungen der beiden Leptonen gesetzt und in Betracht dessen eine Auswahl über die Zuordnung dieser Teilchen zueinander getroffen. Diese Methode wird in ein bereits bestehendes Programm zur kinematischen Rekonstruktion des dileptonischen $t\bar{t}$ Prozesses implementiert und dessen Leistung bezüglich Rechengeschwindigkeit und Qualität der Rekonstruktion anhand verschiedener Parameter vor und nach der Implementierung miteinander verglichen. Dazu wird ein Satz Monte-Carlo-generierter Daten verwendet, aus dem von den beiden Versionen des Programmes Ereignisse dileptonischer $t\bar{t}$ Zerfälle rekonstruiert werden. Letzendlich konnte mit dieser Methode die Rechenzeit stark vermindert werden, ein im Vorfeld erhoffter Gewinn an Qualität der Rekonstruktion konnte jedoch nicht im gewünschten Maße erreicht werden.

Abstract

Due to the relatively good resolution of leptons in particle detectors, the dileptonic $t\bar{t}$ decay seems to be a promising process to get to understand more about the fundamental properties of the top quark. However, the kinematic reconstruction of this decay mode is difficult because of the two neutrinos in its final state, which can not be detected directly in such detectors. Therefore, it is important, to make use of as much information about the involved particles as possible. In this studies, the electromagnetic charge of the jets in the final state of the process is set into relation to the charges of the two leptons and in the respect of that, these particles get assigned to each other. This method gets implemented into an already existing programme for the dileptonic $t\bar{t}$ reconstruction and its performance in quality and processing time is tested on the basis of several parameters before and after the implementation. To do this, a set of Monte Carlo generated data is used, of which events of dileptonic $t\bar{t}$ decays are getting reconstructed by both versions of the programme. As a result, the processing time is reduced heavily, but the anticipated gain in reconstruction quality could not be achieved in the desired way.

Contents

1	Introduction	1
2	Fundamental principles of Particle Physics	3
2.1	The Standard Model of particle physics	3
2.1.1	General structure	3
2.1.2	The top quark	4
2.2	The LHC	7
2.2.1	Layout	7
2.2.2	The ATLAS detector	8
2.2.3	Results of Run I	10
3	Dileptonic $t\bar{t}$ Reconstruction	11
3.1	Fundamental principles	11
3.2	The system of kinematic equations	11
3.2.1	Definition of jet charge	11
3.3	Numerical realization	12
3.3.1	Programme structure	12
3.3.2	Smearing	14
3.3.3	Validation of the jet charge method	15
4	Results	19
4.1	Parameters for performance studies	19
4.2	Performance studies	20
4.2.1	Transverse momentum	20
4.2.2	Pseudorapidity	21
4.2.3	Azimuthal angle	22
4.2.4	Distance	22
4.2.5	CPU time per event	25
5	Conclusion	27

Contents

6	Appendix	29
6.1	Object definition and event selection	29
6.2	Additional plots	30

1 Introduction

The questions, what matter is made of and how does it interact with each other, are of the most interesting questions in modern physics and subject of intensive studies in the scientific community. The concept of indivisible building blocks as the basic level of all existing matter is discussed since several thousands of years and still considered as one of the most promising approaches to the subject. Today, these building blocks are called elementary particles and the most successful theory to describe these particles and their interactions is the Standard Model of particle physics. But since it was not possible to include several physical phenomena like gravity, dark matter and dark energy into this theory, the Standard Model seems to allow space for further improvements, which may come in form of new elementary particles, that were not discovered yet. To search for those, it is necessary to test the existing theories and interactions of particles, that are already included in the Standard Model, as precisely as possible. One way of testing these is to make particles interact by letting them collide with large energies inside of particle accelerators like the Large Hadron Collider (LHC) and then trying to capture as much information about the resulting particles with multi purpose detectors like the ATLAS detector. This procedure allows to produce enormous amounts of experimental data in a very short period of time, making it impossible to evaluate all of the results without the help of computational processing. Therefore it is an important task in particle physics, to write, test and always try to improve programmes, which are capable of evaluating data from such experiments.

The goal of this thesis is, to test the performance of a programme, which is used to reconstruct the kinematics of the so called dileptonic $t\bar{t}$ decay mode and to try to improve it by adding information about the jet charge into the process of reconstruction. The dileptonic $t\bar{t}$ decay mode is one possible process for the top quark t and its anti particle, the antitop quark \bar{t} , to decay into other elementary particles. Since the top quark is to this point the heaviest particle in the Standard Model, which implicates a set of unique properties, that will be described in this thesis, it is particularly interesting to survey this process.

It was hoped-for, to gain an improvement in the quality of the kinematic reconstruction

1 Introduction

by this method and to increase the computing time of the algorithm. The latter goal was achieved in a significant way, while the improvement in the reconstruction quality unfortunately could not have been increased as anticipated.

In the following chapter (Sec. 2), an overview on some of the most important concepts of particle physics, that are crucial to understand the presented studies and build both, the theoretical and the experimental base for it, are presented. Since the LHC is at the moment the only particle accelerator that is able to produce $t\bar{t}$ pairs in a sufficient amount, the experimental side of this chapter focuses mainly on the LHC and in particular on the ATLAS experiment which is native to it, but most of the presented concepts hold also for most of the other accelerators. Sec. 3 gives a deeper understanding on the surveyed dileptonic $t\bar{t}$ process and on the kinematic reconstruction of it. Over the course of it, the numerical realization of the reconstruction process is presented for both, the initial kinematic reconstruction algorithm and the one which was changed by adding information about the jet charge to it. Through out the thesis, the former one will be called *krec* and the latter one will be called *krec + jetch*. In Sec. 4, the methods and results of the performance study of both algorithms is presented and in Sec. 5, a conclusion and an outlook for possible further ways of improvement are shown.

2 Fundamental principles of Particle Physics

2.1 The Standard Model of particle physics

2.1.1 General structure

The Standard Model of particle physics (see Fig. 2.1) is thus far the best description of the fundamental behaviour of the currently known elementary particles. It consists of twelve fermions, four gauge bosons and the Higgs boson, which can interact through three fundamental forces: electromagnetic, weak and strong force. The gravitational force is not a part of the Standard Model since the quantum mechanical properties of it are not yet understood well enough and its impact is negligible at the scale of elementary particles.

The fermions are fundamental spin $\frac{1}{2}$ particles which can be classified by their charges. Charged leptons (e, μ, τ) carry an electromagnetic charge of -1 e and no colour charge, neutrinos (ν_e, ν_μ, ν_τ) carry no charge except the weak, down type quarks (d, s, b) carry an electromagnetic charge of $-\frac{1}{3}$ e and colour charge and up type quarks (u, c, t) carry an electromagnetic charge of $\frac{2}{3}$ e and colour charge. All Fermions carry a weak charge. Another way to divide the fermions in groups is done by classifying them with three generations which differ only in the masses of the embodied particles.

The gauge bosons are the mediators for the three fundamental forces and have a spin of 1. The W and Z bosons embody the weak, the gluon g the strong and the photon γ the electromagnetic interaction. The mathematical formulation of the Standard Model is achieved by a renormalizable quantum field theory based on a local $SU(3) \times SU(2) \times U(1)$ gauge symmetry.

The Higgs boson H can be seen as an excitation of the Higgs field. It carries neither electromagnetic nor colour charge and is the only fundamental particle in the Standard Model with spin 0.

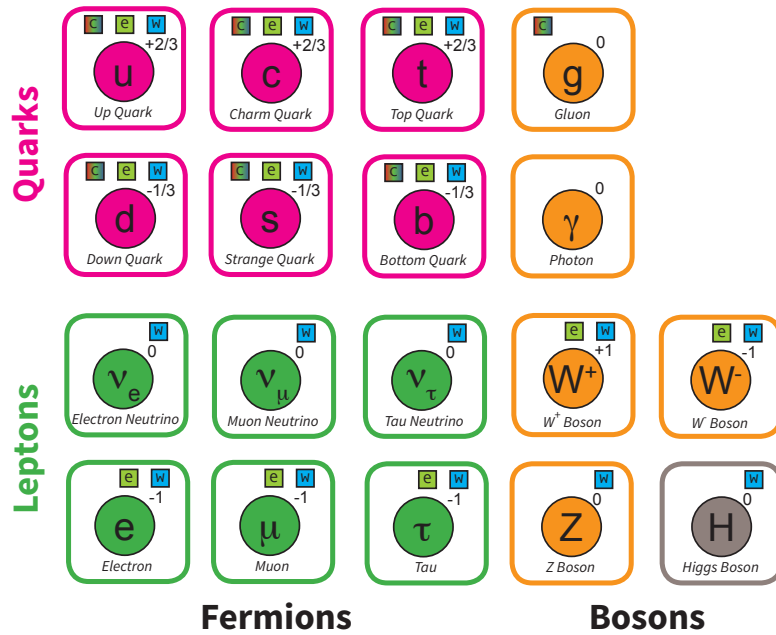


Figure 2.1: Particles of the Standard Model: Leptons (green), quarks (magenta), gauge bosons (orange) and the Higgs boson (grey). The numbers on the upper right of each particle indicate its electromagnetic charge. The boxes on the upper right indicate the fields to which the particle couples: colour (c), electromagnetic (e) and weak (w).

2.1.2 The top quark

Properties

The top quark t is the up-type quark of the third generation. With a rest mass of $m_t = 173.34 \pm 0.27(\text{stat}) \pm 0.71(\text{syst}) \text{ GeV}$ [1], it is the heaviest of all elementary particles in the Standard Model. Like all quarks, it is involved in all fundamental interactions. The top quarks total decay width as predicted by the Standard Model taking NLO and NNLO QCD corrections in account is $\Gamma_t^{\text{theo}} = 1.3 \text{ GeV}$ [2]. An experimental value of $1.10 < \Gamma_t^{\text{exp}} < 4.05 \text{ GeV}$ is given by a direct measurement of the width in Run II of the TEVATRON at FERMILAB [3]. This corresponds (using $\hbar = 6.58211928 \cdot 10^{-16} \text{ eVs}$ [4]) to a mean lifetime of

$$\tau_t^{\text{theo}} = \frac{\hbar}{\Gamma_t^{\text{theo}}} = 5 \cdot 10^{-25} \text{ s},$$

$$5.98 \cdot 10^{-25} \text{ s} > \tau_t^{\text{exp}} > 1.63 \cdot 10^{-25} \text{ s}.$$

These values are one order of magnitude smaller than the timescale needed for hadronization given by [5]

$$\tau_{\text{had}} = \frac{\hbar}{\Lambda_{\text{QCD}}} \approx 3 \cdot 10^{-24} \text{ s.}$$

Therefore, one can conclude that the top quark decays before it hadronizes which is, given that all other quarks can only be observed in bound (hadronized) states, a unique property of the top [6]. As a result, it is possible to measure certain variables that depend on the top quarks spin because it passes its spin information directly on to its decay products. Another interesting property of the top quark is its Yukawa coupling of

$$y_t = \sqrt{2} \frac{m_t}{\nu} \approx 1$$

(using the vacuum expectation value for the Higgs field of $\nu \approx 246$ GeV [4] and the mass m_t as stated above) which makes it a good object of study for Yukawa coupling and hence to understand more about the Higgs mechanism.

Because of these unique properties, the top quark appears to be an excellent candidate to use to perform tests on the Standard Model and to find eventually even physics beyond the Standard Model.

Prediction and discovery

The observation of CP violation in the decay of neutral K mesons by V. Fitch and J. Cronin in 1964 [7] demanded a theoretical explanation. One solution was given by Kobayashi and Maskawa in 1973 [8]. At that time, only two generations of quarks (u , d and c , s) were known, but their explanation of CP violation was only consistent with three (or more) generations. This prediction was further encouraged by the discovery of the τ lepton in 1975 [9] which showed that there are at least three generations of (charged) leptons. Two years later the presence of a third quark generation was proofed by the discovery of the bottom quark by the E288 experiment [10]. In 1995, the existence of the top quark was eventually established by the $D\bar{O}$ and the CDF collaboration at the TEVATRON at FERMILAB by observing $t\bar{t}$ production [11, 12]. As a result, they stated the top mass to be $176 \pm 8(\text{stat}) \pm 10(\text{syst})$ GeV which is consistent with current measurements (see Sect. 2.1.2).

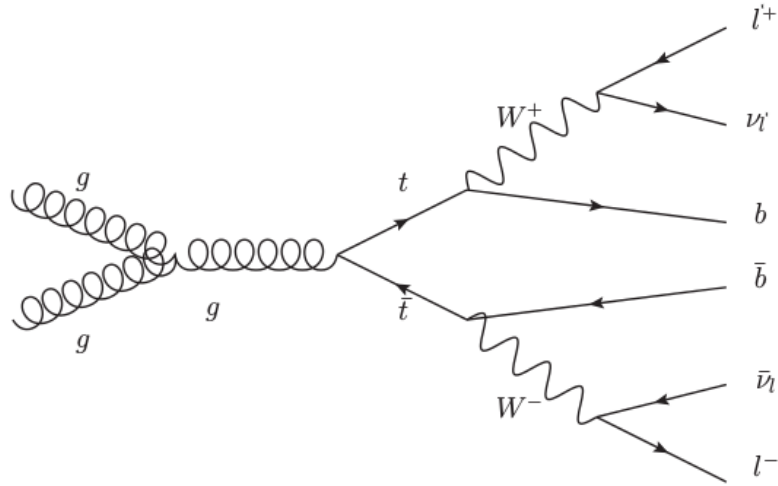


Figure 2.2: The dileptonic decay mode of a $t\bar{t}$ pair produced by gluon fusion (which is the most common $t\bar{t}$ production process in the LHC).

Production and decay

In hadron collisions, top quark pairs $t\bar{t}$ are dominantly produced via $q\bar{q} \rightarrow t\bar{t}$ and $gg \rightarrow t\bar{t}$. TEVATRON being a $p\bar{p}$ collider produces $t\bar{t}$ pairs mainly (85%) via the former process while at the pp collider LHC, which reaches a higher center of mass energy, the latter process plays the leading role (80% at $\sqrt{s} = 7$ TeV and 90% at $\sqrt{s} = 14$ TeV) [4].

Due to its extremely short lifetime, the top quark can only be observed indirectly through its decay products. With a ratio close to 100% it decays via $t \rightarrow W^+q$, where q is a down type quark (d, s, b). Other channels like $t \rightarrow \gamma q$ or $t \rightarrow Zq$, where q is an up type quark other than t (i.e. either u or c), are highly unlikely [4] and would hint at physics beyond the Standard Model. Because of the CKM matrix element $|V_{tb}|$ being close to one, the branching ratio [4]

$$\frac{\Gamma(t \rightarrow W^+b)}{\Gamma(t \rightarrow W^+q)} \approx (0.91 \pm 0.04)\%$$

is also close to 100%. Therefore it is in most of the cases sufficient to consider only $t \rightarrow W^+b$ respectively $\bar{t} \rightarrow W^-\bar{b}$ decays. These kind of decays can be diversified in three categories:

$$\begin{aligned} \text{dijet: } & t\bar{t} \rightarrow W^+W^-b\bar{b} \rightarrow q\bar{q}'q''\bar{q}'''\bar{b}\bar{b} \\ \text{lepton + jet: } & t\bar{t} \rightarrow W^+W^-b\bar{b} \rightarrow q\bar{q}'b\bar{b}l^-\bar{\nu}_l + q''\bar{q}'''\bar{b}\bar{b}l^+\nu_l \\ \text{dileptonic: } & t\bar{t} \rightarrow W^+W^-b\bar{b} \rightarrow l^+\nu_l l'^-\bar{\nu}_l \bar{b}\bar{b} \end{aligned}$$

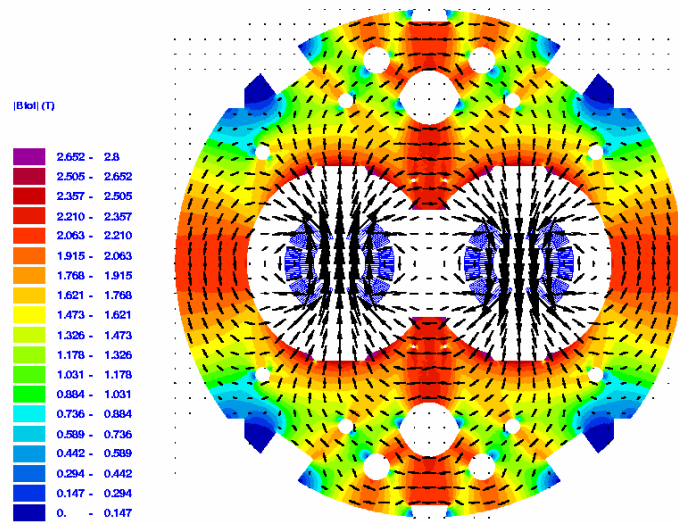


Figure 2.3: Cross section of the beam pipes of the LHC. The coloured portions of the diagram indicate the magnetic flux. The arrows show the magnetic field lines. The two beam pipes are indicated by the blue shaded areas in the middle. One can see that the magnetic field in both tubes is of the same absolute value but points in opposite direction (source: [13]).

In the following, only the dileptonic case (see Fig. 2.2) will be treated.

2.2 The LHC

2.2.1 Layout

After the final shut down of the TEVATRON at FERMILAB in 2011, the LHC (Large Hadron Collider) is presently the only particle accelerator capable of reaching center of mass energies high enough to produce $t\bar{t}$ pairs. The LHC is built to either accelerate protons or fully ionized lead atoms. In the following, I will focus solely on the proton operation mode. In this mode the LHC ran at a center of mass energy of $\sqrt{s} \approx 8$ TeV in Run I and is meant to operate with $\sqrt{s} \approx 13$ TeV after an upgrade, which is planned to be finished this year, in Run II [15].

The protons are obtained from hydrogen gas which gets ionized and than accelerated in the so called booster (see Fig. 2.4). After passing through two smaller preaccelerators (proton synchrotron and super proton synchrotron) they eventually reach the 27 km long beam pipe of the main synchrotron where one half of the protons travels clockwise and the other half anticlockwise. To hold the beams in shape, strong magnetic fields

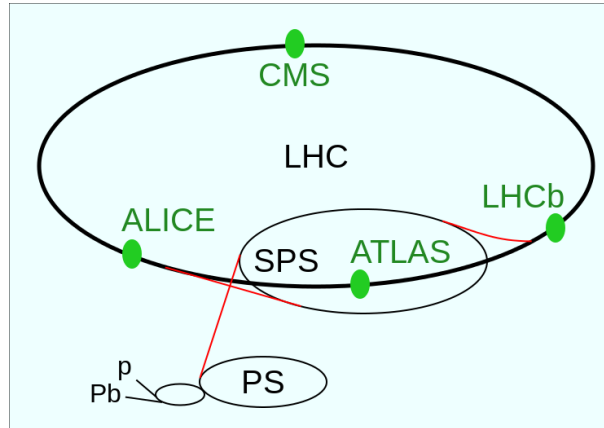


Figure 2.4: The LHC with the four experiments ALICE, ATLAS, CMS and LHCb and the preaccelerators: linear proton accelerator **p**, linear ion accelerator **Pb**, proton synchrotron **PS** and super proton synchrotron **SPS**. The small unmarked ring between the linear accelerators and the **PS** is the booster. The largest ring is the 27 km long main tunnel of the LHC (source: [14]).

are used. These fields must have a very elaborate form to narrow both counterrotating beams simultaneously (see Fig. 2.3). This problem is intrinsic to pp colliders, whereas the opposite charge of the particles in $p\bar{p}$ colliders (like TEVATRON) make it possible to use simpler field geometries. One main advantage of using solely protons is that it is easy to create large numbers of protons from ionizing hydrogen gas which leads to the possibility to obtain a high luminosity, whereas the production of antiprotons in reasonable amounts is very challenging. At several points of the synchrotron, the beam pipes get crossed so that the protons can collide and their decay products can be observed by the detectors that are built around these points (see Fig. 2.4).

2.2.2 The ATLAS detector

The ATLAS detector is one of the four largest experiments at the LHC (see Fig. 2.4). It consists of several layers of detectors that are built around the beam crossing point in the middle (see Fig. 2.5). Strong toroid and solenoid magnets (see Fig. 2.6) are used to bend the particle's trajectories, making it possible to get information about the particles properties from the curvatures of the corresponding tracks.

The central tracking system of ATLAS is formed by silicon pixel detectors, silicon microstrips (SCT), and straw drift chambers with transition radiation function which are surrounded by a 2 T superconducting solenoid magnet [18]. When an electrically charged particle enters a pixel or microstrip of the silicon detectors, it ionizes some of the embodied silicon atoms, creating electron hole pairs which can be read out as an electronic

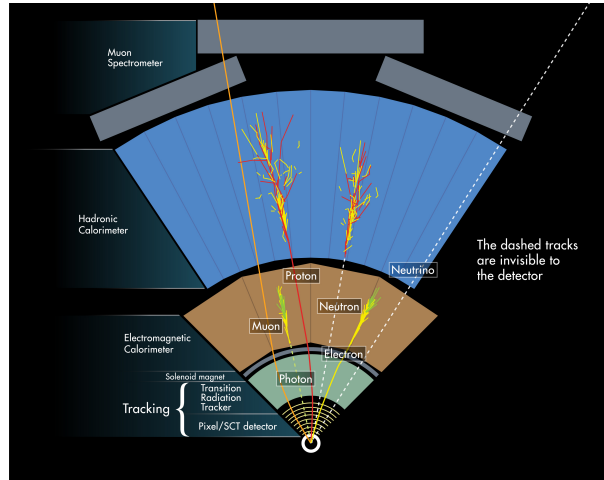


Figure 2.5: Schematic structure of the different types of detectors used in the ATLAS experiment. The particle tracks represent in which detector such kind of particles are most of the time detected respectively which part of the detector the particles pass through without leaving any signal (dashed lines) (source: [16]).

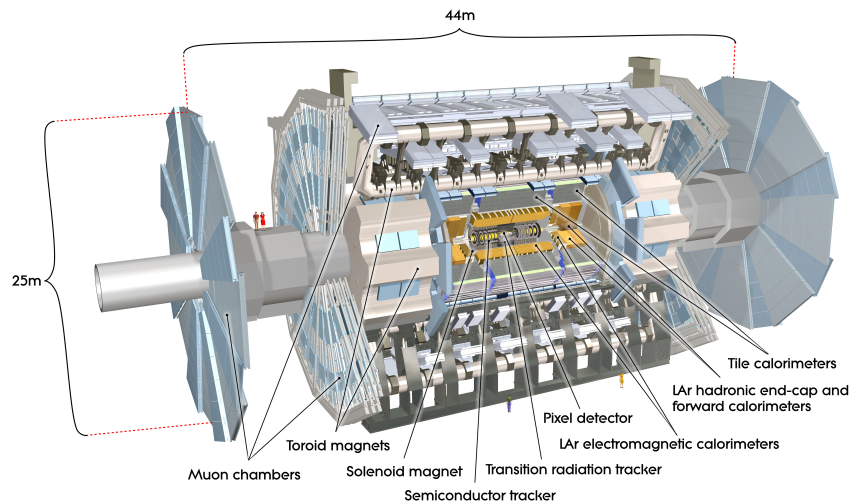


Figure 2.6: Graphical representation of the structure of the ATLAS detector. On the left hand side one can see two humans for scale (source: [17]).

signal. Since the exact positions of all pixels and microstrips in the detector are known, it is possible to reconstruct a particles trajectory out of these signals.

A transition radiation tracker contains several layers of material with different indices of refraction. Since the propability of a particle producing transition radiation is dependent on its Lorentz factor, latter can be obtained by measuring the intensity of the radiation. With given energy and Lorentz factor, it is possible to calculate the mass of the particle. The central tracking system is surrounded by the electromagnetic calorimeter. This component consists of sensing material in which penetrating charged particles can dispense their energy via ionization and bremsstrahlung. These energies can be read out and then matched to particle tracks of the central tracking system. In the inner sections of the calorimeter liquid argon is used as sensing material whereas in the outer region scintillating tiles of plastic are used.

The hadronic calorimeter surrounds the electromagnetic calorimeter. In this component, the particles deposit their energy dominantly via the strong interaction, making it able to detect particles which are not necessarily electrically charged.

The most outer part of ATLAS consists of muon chambers, which provide additional data on the particle tracks for muons that did not deploy their whole energy in the calorimeters. Because of this it is possible to obtain a higher resolution on the very small curvatures of such tracks. On the endcaps of the ATLAS experiment there are are also two large round plates consisting of muon chambers (see Fig. 2.6). These are used to detect trajectories of muons with large pseudo rapidities.

2.2.3 Results of Run I

LHC Run I was meant to provide data to test the predictions of the Standard Model and physics beyond. One of the main aims was to confirm the existence of the Higgs boson, being until 2012 the only particle of the Standard Model which was not experimentally validated. In July 2012 the ATLAS and the CMS collaboration declared with 5 sigma significance the discovery of a boson in the mass region of 125–126 GeV which is consistent with theoretical predictions about the Higgs boson [19, 20]. Although it seems very clear that this particle is in the predicted mass range and is indeed a boson, it is not debarred yet that this particle might differ in other properties from the Higgs boson. Therefore, more research has to be done and it is expected to retrieve more information from Run II. One other aim of Run I was the search for supersymmetry. Until now, the LHC was not able to offer sufficient proof for the existence or absence of supersymmetrical particles but for many hypothetical particles certain mass regions had been excluded (e.g.: [21]), paving the way for future research on this topic in Run II.

3 Dileptonic $t\bar{t}$ Reconstruction

3.1 Fundamental principles

3.2 The system of kinematic equations

Neutrinos have neither electromagnetic nor colour charge, making it impossible to detect them directly in particle detectors. One way to deal with this problem is to look for missing transverse momentum in detected particle trajectories. But this method fails if there are two (or more) neutrinos involved because it is not trivial to determine which fraction of the missing momentum belongs to which particle. Since there are two neutrinos in the final state of the dileptonic $t\bar{t}$ decay (see Sect. 2.1.2) it is impossible to reconstruct its complete kinematics. Determining the four vectors of the t quark and the \bar{t} quark in this process is therefore as trying to solve the following underconstrained system of equations [22].

$$p_b + p_{W^+} = p_t \tag{3.1}$$

$$p_{\bar{b}} + p_{W^-} = p_{\bar{t}} \tag{3.2}$$

$$p_{t^+} + p_\nu = p_{W^+} \tag{3.3}$$

$$p_{t^-} + p_{\bar{\nu}} = p_{W^-} \tag{3.4}$$

$$p_{\nu_x} + p_{\bar{\nu}_x} = E_x^{\text{miss}} \tag{3.5}$$

$$p_{\nu_y} + p_{\bar{\nu}_y} = E_y^{\text{miss}} \tag{3.6}$$

But by making certain assumptions on the properties of the involved particles, it is possible to solve the system. Therefore (in the style of [22]), the masses of the top quark, the W boson and all neutrinos were set to $m_t = 172.5$ GeV, $m_W = 80.4$ GeV and $m_\nu = 0$.

3.2.1 Definition of jet charge

Since particles which carry a colour charge (e.g. quarks), interact via the strong force, it is not possible to detect them directly. This is because of the QCD confinement, which

3 Dileptonic $t\bar{t}$ Reconstruction

says that such particles cannot exist in unbound states and will always tend to form colourless bound states with other particles. An unbound state of a particle with colour charge would be equal to the effect of another particle with colour charge in an infinitely distance which implies a therefore infinite strong force to the first particle. This effect results from the unique property of the strong force to increase with increasing distance. As a result, such particles hadronize inside the detector due to further emission of photon and gluon radiation form so called jets. These are sprays of non elementally hadrons which can be detected and can give indications of the properties of the particle from which the individual jet emerged. Because of the boost of the primary particle, such jets mostly have the form of narrow cones.

In a detector jets appear in the form of several tracks of particles and energy deposition in the calorimeters. Such a track is counted as part of a jet if $\Delta R(\text{jet axis, track}) < 0.35$, where $\Delta R := \sqrt{\Delta\varphi^2 + \Delta\eta^2}$. The jet axis is the middle axis of the cone which forms the jet. It is now possible to define a weighted jet charge which gives certain information about the charge of the initial particle from which the jet emerged. Based on [23], the definition used in the following is

$$q_{\text{jet}} = \frac{\sum_i q_i |\vec{j}\vec{p}_i|^k}{\sum_i |\vec{j}\vec{p}_i|^k}, \quad (3.7)$$

where q_i is the charge of the particle which forms a certain track i and \vec{p}_i the corresponding momentum. \vec{j} is the mean momentum of the jet and k is a weighing factor which is set to $k = 0.5$. This way of defining the properties of a jet is in the style of [24].

3.3 Numerical realization

3.3.1 Programme structure

The goal of this bachelor thesis was, to implement information about the weighted jet charge (see Sect. 3.2.1) into an already existing algorithm for the reconstruction of the dileptonic $t\bar{t}$ decay. The used algorithm corresponds to the kinematic reconstruction method described in [22], where the system of equations shown in Sec. 3.2 has to be solved numerically. To do this, the numerical Newton-Raphson method is used.

krec takes as a first step the four momenta of the leptons and jets and the missing transverse energy from the neutrinos from an input tree (see Fig. 3.1 [left]). Because it is

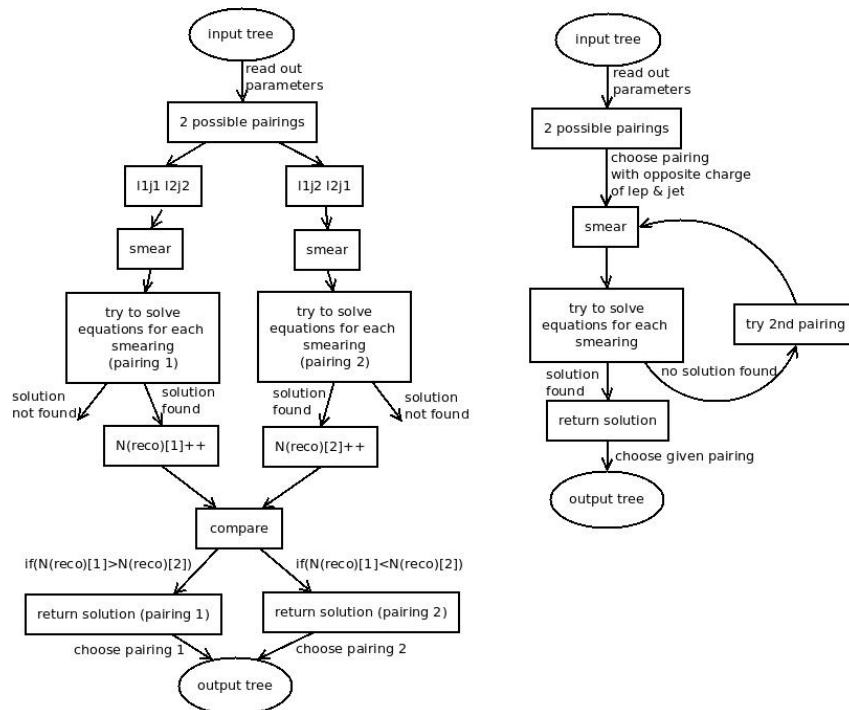


Figure 3.1: Flow chart of the structure of the programme for the kinematic reconstruction of the dileptonic $t\bar{t}$ decay before the implementation of jet charge ($krec$) [left] and the structure of the programme after the implementation of jet charge ($krec + jetch$) [right].

not known from the beginning which of the jets corresponds to the b quark and which one to the \bar{b} quark in the final state of the decay process (see Fig. 2.2), both possible pairings (lepton 1 \rightarrow jet 1 and lepton 2 \rightarrow jet 2 [in the following called $l1j1$] or lepton 1 \rightarrow jet 2 and lepton 2 \rightarrow jet 1 [in the following called $l1j2$]) have to get reconstructed. The jet with the higher transverse momentum p_T is called jet 1 whereas lepton 1 is simply the lepton which is stored first in the input tree.

The four momenta of the leptons and jets and the missing transverse energy underlie experimental uncertainties. Therefore, it is necessary to smear these parameters as described in Sec. 3.3.2. smearing is done N_{smear} times and in each of this times the four momenta of the jets and the missing transverse energies are set to a different value in the range of the given resolution around the input initial values of this parameter. Then the system of equations (see Sec. 3.2) is tried to get solved numerically for this parameters. This is done for both possible pairings $l1j1$ and $l1j2$. Every time, a solution is found for one of the given pairings and smeared parameters, a counter N_{reco}^1 (for $l1j1$) or N_{reco}^2 (for $l1j2$) gets raised by one. After running over all N_{smear} different sets of smeared parameters for both pairings, the counters N_{reco}^1 and N_{reco}^2 are compared and the pairing with the larger counter (i.e. the pairing for which the most solutions were found) gets selected and

3 Dileptonic $t\bar{t}$ Reconstruction

for this pairing the parameters of the reconstructed jets, leptons and neutrinos together with the parameters of their mother particles (W^\pm and t, \bar{t}) are written into the output tree. It is also possible that there are no solutions found for any of the two pairings. In this case, the event could not have been reconstructed. The number of smearings (see Sec. 3.3.2) is set to $N_{\text{smear}} = 500$ in all of the studies.

The system of equations can have up to four real solutions. Therefore it is possible that the algorithm finds more than one solution for one given set of smeared parameters and pairing. In this case the solution with the lowest effective mass $m_{t\bar{t}}$ of the $t\bar{t}$ system is taken. This is done because the $t\bar{t}$ cross-section decreases with the centre of mass energy s and therefore also with the effective mass $m_{t\bar{t}}$ [22]. Because of that, the probability for $t\bar{t}$ production with lower effective mass $m_{t\bar{t}}$ is larger. For efficiency reasons, the programme actually stops after finding two solutions. This is done because in most of the cases (a few percentages) there are not more than two solutions for the system and searching for more would lead to much more processing time but no big gain in terms of reconstruction quality [22].

krec+jetch uses the same input data as *krec* but in addition takes the jet charges (see Sec. 3.2.1) into account. This is done by matching the two jets to the two leptons in such a way, that the jet with the larger (signed) charge gets matched to the lepton with the smaller (signed) charge (in this case -1 , because the lepton charges in the input sample always have the discrete values ± 1). This pairing is then defined as l1j1. For this pairing the process of smearing and solving of the system of equations is done in the same way as in the current programme. The difference to *krec* is, that for the beginning this process has to be done only for one pairing (l1j1) and not for both. Only if for the first pairing there is no solution found at all (for any of the N_{smear} samples of smeared parameters), the process gets repeated for the second pairing l1j2. After that, if there was a solution for l1j1 found, it gets written into the output tree in the same way as in *krec*. If there was no solution for l1j1 but for l1j2, the solution for l1j2 gets written into it.

3.3.2 Smearing

Since the measurement of the kinematic parameters of particles in detectors underlays certain inaccuracies, it is necessary to smear these parameters according to their resolutions. This means, the reconstruction of one set of kinematic parameters does not get done only once but gets repeated several times, whereby in every iteration, the parameters are changed to different values inside the range of the detector resolution of these parameters.

To calculate the detectors efficiency for the transverse momenta reconstruction, the value

$$\frac{p_T^{\text{truth}} - p_T^{\text{rec}}}{p_T^{\text{truth}}}$$

was filled in a histogram per bin of p_T . For the resulting histogram, a combination of two Gaussians was used as fitting function, since the histograms are not symmetrical and therefore a single Gaussian fit would not have been sufficient. The asymetry of the resolution of p_T can be seen in Fig. 6.8 and will be discussed further in Sec. 4.2.1.

To calculate the missing energy resolutions,

$$\sum_{\text{neutrinos}} p_T^{x/y} - E_T^{x/y,\text{miss}}$$

was plotted for both, x - and y - direction, and then both histograms were fitted with a single Gaussian each. This way of determining the resolution functions is in the style of [22] and based on the way of determining the transfer functions in [25]. As suggested in [22], only the transverse momenta of the jets and the missing energy of the neutrinos were smeared. The resolutions for the momenta of the leptons would be very much smaller than for the jets, and therefore smearing the leptons would cause an increase in processing time and would not have a big impact on the quality of the reconstruction.

3.3.3 Validation of the jet charge method

Before implementing the jet charge as a criterion on how to match the jets to the leptons in the programme, it is necessary to determine, whether it is possible to deduce which of the two jets in the sample corresponds to the b and which to the \bar{b} quark, only by looking at the jet charges. In theory, the charges of a b jet should be smaller than the one of a \bar{b} jet, since a b , being a down type quark, has a negative charge of $-\frac{1}{3}$ and a \bar{b} being the antiparticle to the b , has a positive charge of $+\frac{1}{3}$.

This can be seen in Fig. 3.2, were the charges of the two generated jets were entered. The mean value of the histogram for the b jet charge of -0.093 is obviously smaller than the mean value of the histogram with the \bar{b} jet charges of $+0.097$. But the separation of the two histograms is very small and there is a large overlap between them. Therefore, there is some doubt, whether the jet charge is a reliable parameter for choosing the pairing of leptons and jets correctly. As a result, it is for some events possible, that, even though the jet and lepton charges suggested a certain jet lepton pairing, the other possible pairing would actually be the right one. Therefore, in the implementation of the jet charge as it can be seen in the flowchart in Fig. 3.1, it was necessary to try to reconstruct the

3 Dileptonic $t\bar{t}$ Reconstruction

kinematics for the second pairing every time there was no solution found for the first one. Otherwise a lot of events would be lost and counted as not reconstructed.

One reason for the small separation of charges is obviously the relatively small absolute value of the charge of down type quarks and antiquarks like b and \bar{b} . Another cause lays in the measuring mechanism of the weighted jet charge as described in Sec. 3.2.1. Tracks (and therefore their charges) do not get counted if they are outside of the jet cone. The definition of the cut at $\Delta R = 0.35$ is empirically motivated and different cutting points would cause different values for the jet charges. This holds also for the weighing factor $k = 0.5$.

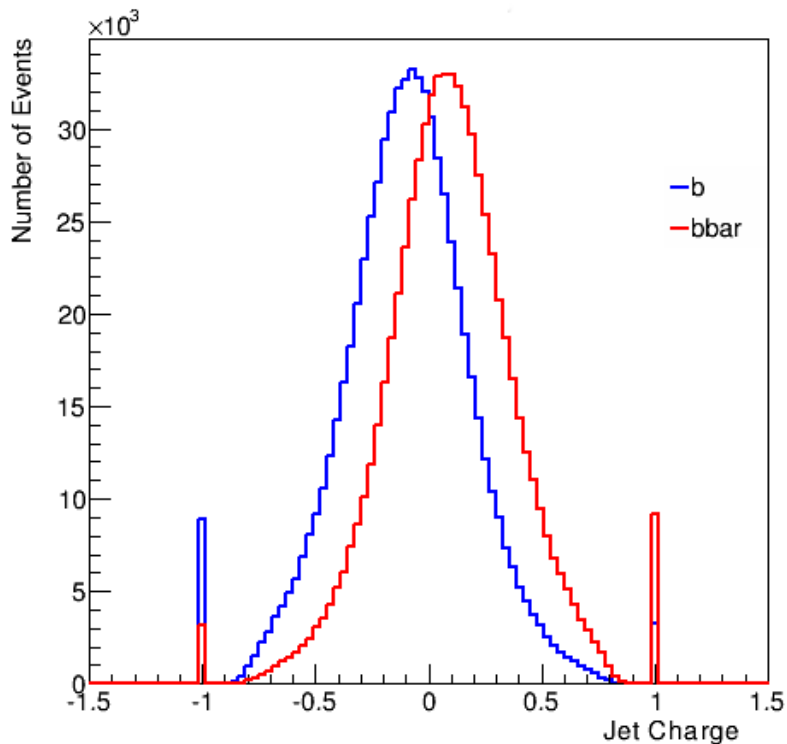


Figure 3.2: Jet charges on generated level. The two jet charges for every event were associated as b and \bar{b} according to which of the corresponding jets was closer (smaller ΔR (see Sec. 4.1 for a definition)) to the generated b or \bar{b} . The peaks at ± 1 are an effect of the definition of the jet charge as it is given in Eqn. 3.7. Since quarks can not be detected directly due to hadronization, the tracks that are inside the jet cone can only come from particles with charges of $q_i = 0, \pm 1$. Looking at the equation shows, that the weighted jet charge is $+1$ for every jet that consists solely out of tracks with charges of $+1$ and 0 and $+1$ for jets that consist solely out of tracks with charges of -1 and 0 .

4 Results

4.1 Parameters for performance studies

To compare the performance of the *krec+jetch* to *krec*, there are a variety of parameters to look at. To do this, certain properties of the particles have to be looked at on both, the generated (gen) and reconstructed (rec) level. The former one describes the properties as they are in the Monte Carlo generated sample before reconstruction and therefore could also be called truth values, whereas the latter one describes the properties after the reconstruction with *krec* or *krec+jetch*. The definition of the parameters as well as the choice of the histograms to produce and evaluate was inspired by [22], but more different parameters and histograms were added, which may allow a deeper look at the topic. Both programmes were tested on the same sample of Monte Carlo generated events (see Sec. 6.1 for object definition and event selection). In the following, the parameters used in the performance studies get defined.

Distance: The distance of two particles is defined as $\Delta R(a, b) := \sqrt{\Delta\varphi^2 + \Delta\eta^2}$. Here $\Delta\varphi := (\varphi_a - \varphi_b)$ modulo 2π is the difference of the azimuthal angle of the first particle a and the second particle b . $\Delta\eta := \eta_a - \eta_b$ is the difference of the pseudorapidity of particle a and particle b . It cannot only be calculated for two particles that are in the same event and reconstruction level. It is for example also useful to look at the distance between a reconstructed particle and a generated one.

Resolutions: The resolution of a parameter a is defined as the non fitted Root Mean Square (in the following RMS) of the histogram of the differences of $a_{\text{reco}} - a_{\text{gen}}$.

Average CPU time per event: The arithmetic average of the CPU time that is needed to pass the whole reconstruction process for one event of the input sample.

4.2 Performance studies

4.2.1 Transverse momentum

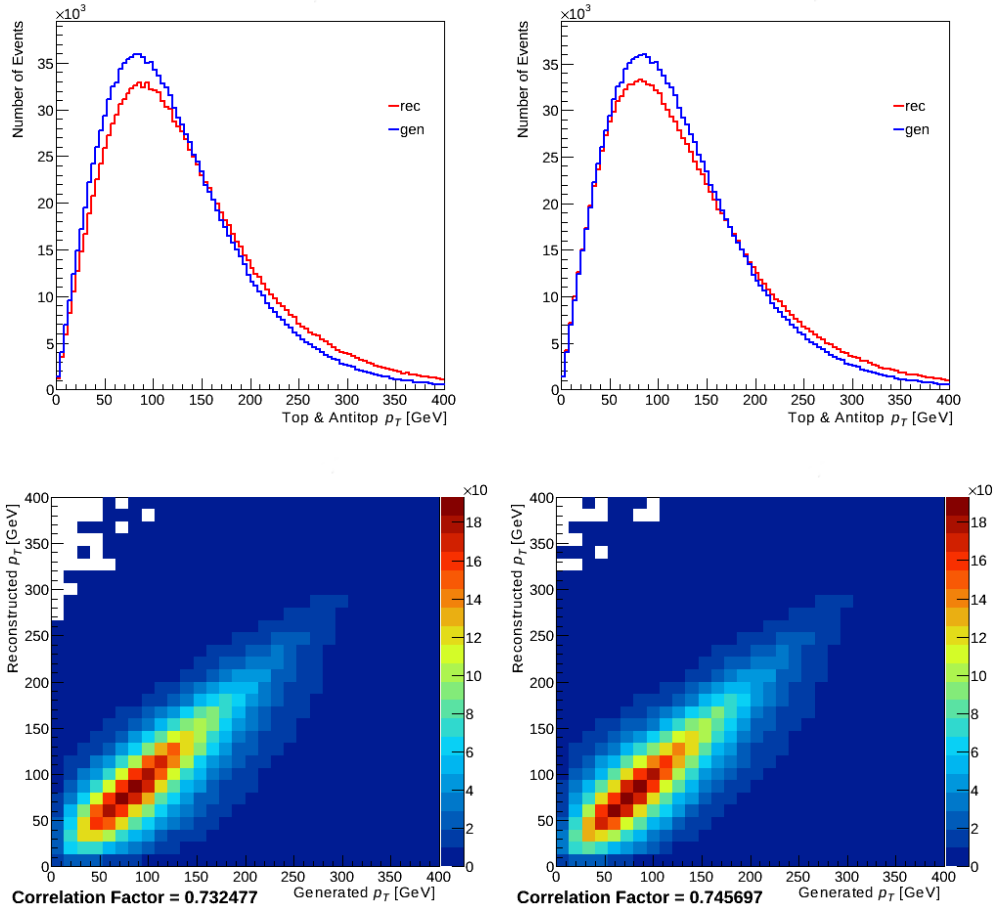


Figure 4.1: Transverse momentum p_T for t and \bar{t} filled in the same histograms at reconstructed (rec) and generated (gen) level for $krec$ [left] and $krec + jetch$ [right]. Top row: p_T distributions. Bottom row: Reconstructed over generated p_T .

The reconstructed transverse momentum p_T (rec) appears to be shifted to higher values (see Fig. 4.1) in both, the original and the one after the implementation of the jet charge. This effect shows similarly for t (Fig. 6.1), \bar{t} (Fig. 6.2) and therefore also for the $t\bar{t}$ system (Fig. 6.3). This can be seen even better in the resolution plots (Fig. 6.8, 6.9, 6.10 and 6.11). Here are the resolution curves obviously not symmetrical and also shifted to positive values. This effect seems to be stronger for $krec$, which can be seen by the mean values of the resolution histograms for transverse momenta represented in Tab. 4.1. All mean values for p_T (except the one for the $t\bar{t}$ system) concerning $krec + jetch$ appear

to be smaller than the ones for $krec$. This indicates that the reconstructed transverse momenta for $krec + jetch$ are closer to the generated values than they are for $krec$. That is also shown in the correlation plots for the transverse momentum (Fig. 4.1, 6.19 and 6.20). In all of these plots the correlation factor is higher for $krec + jetch$.

4.2.2 Pseudorapidity

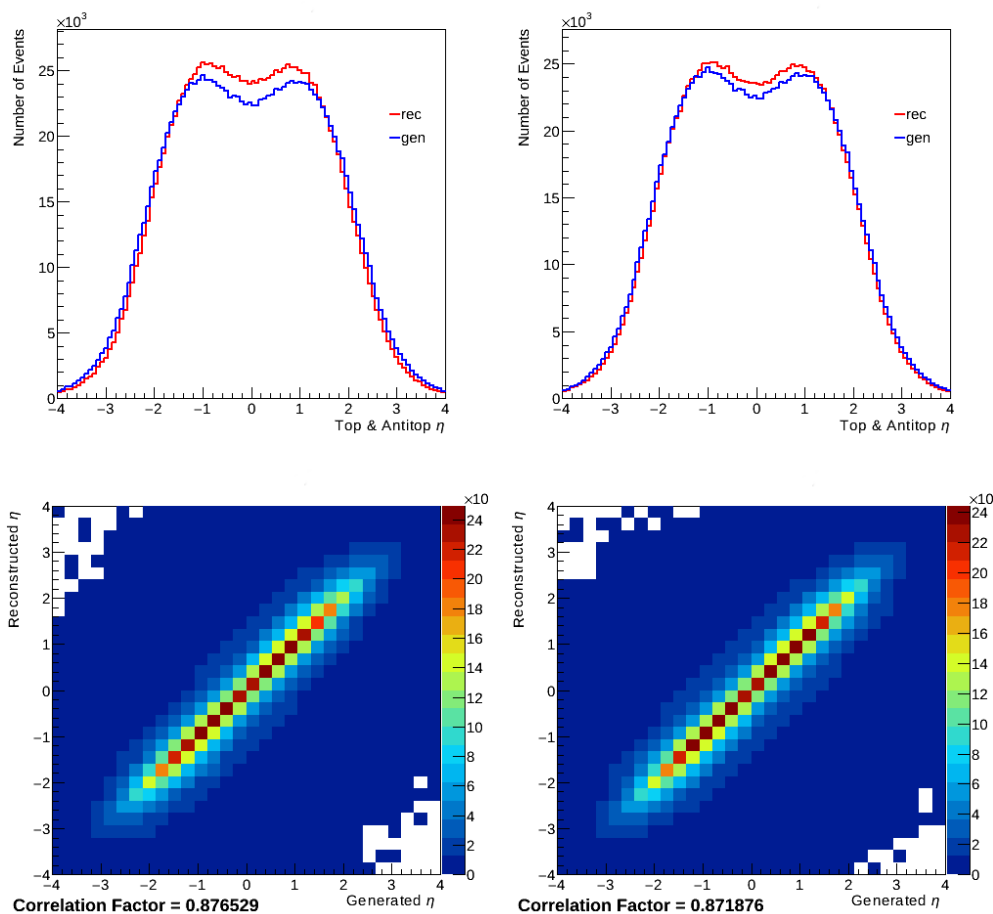


Figure 4.2: Pseudorapidity η for t and \bar{t} filled in the same histograms at reconstructed (rec) and generated (gen) level for $krec$ [left] and $krec + jetch$ [right]. Top row: η distributions. Bottom row: Reconstructed over generated η .

In both, $krec$ and $krec + jetch$, the reconstructed pseudorapidity η tends to have slightly smaller absolute values than the generated one. This becomes apparent in the Fig. 4.2 for both, t and \bar{t} together, 6.4 for (t) and 6.5 for \bar{t} . As it is shown in Tab. 4.1, the resolutions of η are slightly higher for the $krec + jetch$. That means that the reconstructed values match the generated values slightly worse for this programme and settles also in the lower

Parameter	Histogram	Mean [old]	Mean [new]	RMS [old]	RMS [new]
p_T [GeV]	t and \bar{t}	14.06	9.70	59.64	58.11
	t	14.10	9.74	59.65	58.08
	\bar{t}	14.02	9.65	59.63	58.13
	$t\bar{t}$ system	10.36	12.30	23.56	25.20
η	t and \bar{t}	$8.82 \cdot 10^{-4}$	$9.50 \cdot 10^{-4}$	0.76	0.78
	t	$-2.96 \cdot 10^{-4}$	$7.24 \cdot 10^{-4}$	0.76	0.78
	\bar{t}	$2.06 \cdot 10^{-3}$	$1.18 \cdot 10^{-3}$	0.76	0.78
	$t\bar{t}$ system	$4.80 \cdot 10^{-3}$	$4.80 \cdot 10^{-3}$	1.42	1.43
φ	t and \bar{t}	$5.36 \cdot 10^{-4}$	$1.16 \cdot 10^{-4}$	0.86	0.88
	t	$2.07 \cdot 10^{-3}$	$9.50 \cdot 10^{-4}$	0.86	0.88
	\bar{t}	$-9.96 \cdot 10^{-4}$	$-7.18 \cdot 10^{-4}$	0.86	0.88

Table 4.1: Not fitted RMS and mean values of the histograms for the resolution of the transverse momentum p_T , pseudorapidities η and azimuthal angle ϕ of t and \bar{t} filled in the same histograms, t , \bar{t} and the $t\bar{t}$ system for *krec* [old] and for *krec + jetch* [new]. The corresponding histograms can be seen in Fig. 6.8, 6.9, 6.10 and 6.11 for p_T , Fig. 6.12, 6.13, 6.14 and 6.15 for η and Fig. 6.16, 6.17 and 6.18 for φ .

correlation factors in the correlation plots Fig. 4.2, 6.21 and 6.22 in opposite to the old programme.

4.2.3 Azimuthal angle

Since there is no physical effect, that would result in any kind of preference of values for azimuthal angles φ , the distribution of it should be a flat line in the interval $[-\pi, \pi]$ for the reconstructed as well as the generated values. This is the case for both programmes, as it can be seen in figure 4.3, 6.6 and 6.7. However, the resolutions (RMS) of φ shown in Tab. 4.1 are bigger and therefore worse for *krec+jetch*. This also holds for the correlation plots 4.3, 6.23 and 6.24, which show larger correlation factors for the old programme.

4.2.4 Distance

The distance $\Delta R(a, b)$ between two particles a and b , as defined in Sec. 4.1, indicates whether the particles have similar directions in the detector. It stands to reason that one can look at the distance between a generated particle and the particle that was reconstructed as it. Since ΔR is dependent on both, the difference of pseudorapidity $\Delta\eta$ and the difference of azimuthal angle $\Delta\varphi$, it is a good indicator in whether the particles were reconstructed correctly. In this case the generated and reconstructed particles must have a small distance to each other. In the following, fractions of the number of reconstructed

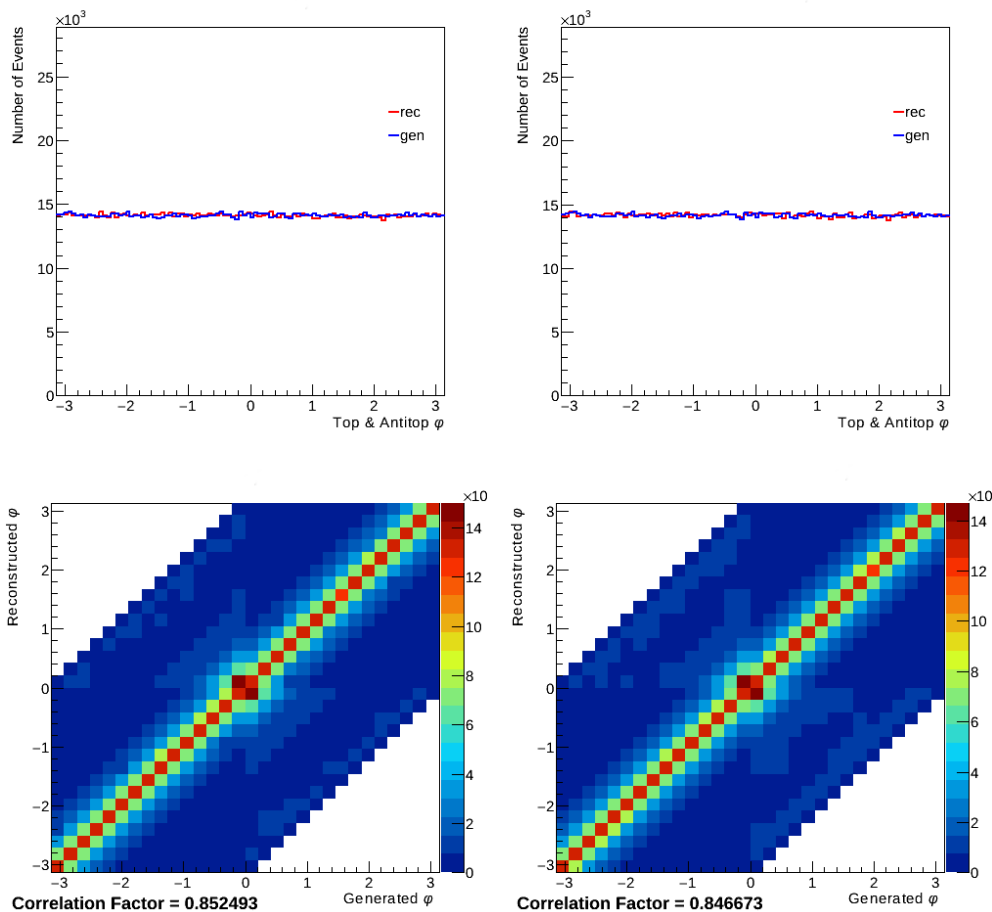


Figure 4.3: Azimuthal angle φ for t and \bar{t} filled in the same histograms at reconstructed (rec) and generated (gen) level for $krec$ [left] and $krec + jetch$ [right]. Top row: φ distributions. Bottom row: Reconstructed over generated φ .

events that pass certain conditions over the number of all reconstructed events in the sample will be observed. In the style of the performance studies presented in [22], the conditions regard, whether two particles have a distance $\Delta R < 0.3$. They are shown in Tab. 4.2.

For condition 1 $krec + jetch$ (see Tab. 4.2 for the definition of the conditions) $krec + jetch$ performs worse than $krec$, showing a difference of 0.55%. This may be attributed to the difference in the programmes in finding the final pairing of leptons and jets. As described in Sec. 3.3.1, in the original version both possible pairings get checked for every event and then the final one gets chosen by the number of solutions that were found for the different pairings. On the contrary, in $krec + jetch$, one pairing gets chosen at first and the other pairing only gets checked, if there was no solution at all for the first pairing. Therefore it is possible that for example there is only one solutions for the first pairing but there

4 Results

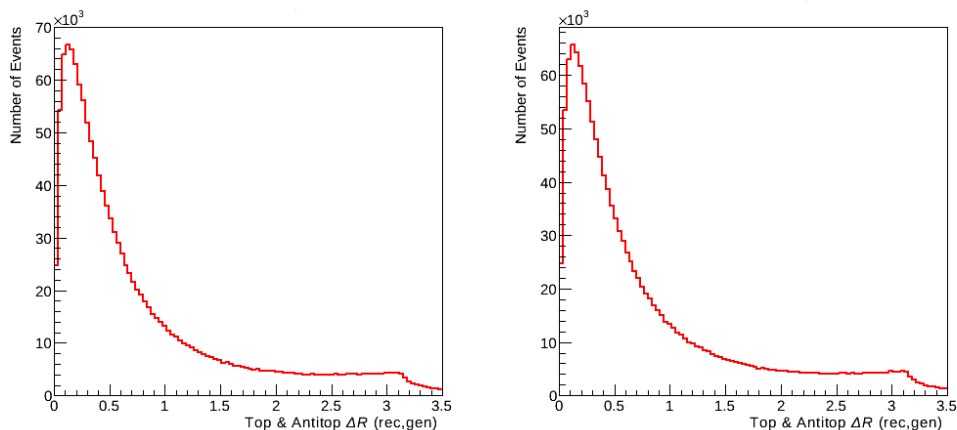


Figure 4.4: $\Delta R := \sqrt{\Delta\varphi^2 + \Delta\eta^2}$ between reconstructed and generated t and \bar{t} filled in the same histograms for $krec$ [left] and $krec + jetch$ [right].

would be much more solution for the other one, if it would have been checked. In this case the second pairing would be a more probable candidate of being the right one, but would still be omitted by the algorithm. This decrease in reconstruction quality seems to be inevitable if one wants to increase the running speed (lower CPU time per event) of the programme by using the introduced method of implementing jet charge.

A graphical representation of this condition is given in Fig. 4.4, 6.25 and 6.26. All events that are in both, the histogram of figure 6.25 and the histogram in Fig. 6.26, in bins on the left side of 0.3 ($\Delta R < 0.3$), fulfil condition 1 and therefore contribute to a higher percentage in this category. In all of the three figures, there is an apparent shoulder at $\Delta r \approx \pi$. This can be explained as an effect of wrongly reconstructed events, where the reconstructed azimuthal angle φ of the t is close to the generated φ of the \bar{t} and vice versa. Due to conservation of momentum, the t and \bar{t} tend to fly in opposite azimuthal directions in the detector. As a result, the reconstructed and generated t (\bar{t} respectively) are back to back and therefore show a difference in azimuthal angle of $\Delta\varphi \approx \pi$. For $\Delta\eta \approx 0$ this would result in $\Delta R \approx \pi$ and therefore contribute to the shoulder. It is also possible that $\Delta\eta$ shows similar values to π . The distribution of the pseudorapidity η has two maxima at values near to $\pm\frac{\pi}{2}$ (see Fig. 4.2), which would result in $\Delta\eta \approx \pi$ for events where the pseudorapidity of the generated and the reconstructed t (\bar{t} respectively) are close to the two different maxima¹. With $\Delta\varphi \approx 0$ this would also lead to $\Delta R \approx \pi$. Condition 2 indicates, if both reconstructed jets are close to the generated jets, without

¹Notice, that a pseudorapidity of $\eta \approx \pm\frac{\pi}{2}$ would correspond to an angle of $\theta = 2\arctan(e^{-\frac{\pi}{2}}) = 0.41 = 23.47^\circ$. Therefore the fact that the maxima in η are close to $\approx \pm\frac{\pi}{2}$ has no deeper physical reason and the connection to π is just arbitrary here. This is a contrast to φ , where $\Delta\varphi = \pi$ was the physical result of the particles being exactly back to back.

considering if they were matched correctly (which would be b_{rec} to b_{gen} and \bar{b}_{rec} to \bar{b}_{gen}). *krec + jetch* performs slightly worse in this condition, but only with a small deviation of 0.02%. Since this condition does not imply, whether the jets were matched correctly as b or \bar{b} , it would not have been expected, if the *krec + jetch* would have performed better in this category. This is, because the utilisation of jet charge should mainly take impact on the correctness of matching the jets to b and \bar{b} but not necessarily on whether the jets are close to any of the generated b or \bar{b} without distinguishing between them.

Conditions 3 to 8 are dependent on the correct matching of the jets to the generated b and \bar{b} . Therefore, *krec + jetch* should show a better performance in this categories. This is actually the case, since the percentages for it are higher for the conditions 3 to 5 (which indicate right matching) and lower for the conditions 6 to 8 (which indicate wrong matching).

4.2.5 CPU time per event

The CPU time per event for *krec + jetch* is with 0.45 s significantly shorter than for *krec* with 4.06 s. One reason for that large decrease is, that in *krec* for every event both possible pairings of jets to leptons are tried to get reconstructed and only after that, one of the pairings is chosen to be the final pair. In *krec + jetch* one of the pairings gets to be chosen by looking at the jet charges and lepton charges before trying to reconstruct it and therefore, the second pairing only has to be reconstructed when no solution has been found for the first one. As a result, in the latter programme, the reconstruction algorithm has to be passed through not as often for the same sample of events.

Condition	old	new
1: $\Delta R(t_{\text{rec}}, t_{\text{gen}}) < 0.3$ and $\Delta R(\bar{t}_{\text{rec}}, \bar{t}_{\text{gen}}) < 0.3$	20.59%	20.04%
2: ($\Delta R(b_{\text{rec}}, b_{\text{gen}}) < 0.3$ or $\Delta R(b_{\text{rec}}, \bar{b}_{\text{gen}}) < 0.3$) and ($\Delta R(\bar{b}_{\text{rec}}, b_{\text{gen}}) < 0.3$ or $\Delta R(\bar{b}_{\text{rec}}, \bar{b}_{\text{gen}}) < 0.3$)	94.58%	94.56%
3: condition 2 and $\Delta R(b_{\text{rec}}, b_{\text{gen}}) < 0.3$	78.92%	79.30%
4: condition 2 and $\Delta R(\bar{b}_{\text{rec}}, \bar{b}_{\text{gen}}) < 0.3$	78.92%	79.30%
5: condition 3 and condition 4	78.89%	79.26%
6: condition 2 and $\Delta R(b_{\text{rec}}, \bar{b}_{\text{gen}}) < 0.3$	15.67%	15.27%
7: condition 2 and $\Delta R(\bar{b}_{\text{rec}}, b_{\text{gen}}) < 0.3$	15.67%	15.27%
8: condition 6 and condition 7	15.63%	15.23%

Table 4.2: Fractions of reconstructed events that fulfil the conditions 1 to 8 over the number of all reconstructed events in the sample for *krec* [old] and the *krec+jetch* [new]. The definitions of the conditions 1 to 8 are given in the left column.

5 Conclusion

As shown in section 4.2.1, 4.2.2 and 4.2.3, the anticipated gain in the quality of the reconstructed kinematic parameters was not achieved. This may be an effect of the relatively small separation of b and \bar{b} jet charges (Sec. 3.3.3), making them a questionable parameter for a distinct indicator to determine the correct pairing of jets to lepton numbers. Even though, the resolution of the transverse momentum p_T of t and \bar{t} was slightly lower for $krec + jetch$ than for $krec$, the two other kinematic parameters η and φ showed slightly higher resolutions for $krec + jetch$. That was further proven by looking at the correlation factors between the reconstructed and the generated level of these values for both versions of the programme. By the distance of the reconstructed t and \bar{t} to the generated ones (Sec. 4.2.4), it was also shown, that the quality of reconstruction of the kinematic parameters slightly decreased by adding the jet charge to the algorithm. But by looking at the distances of the b and \bar{b} on generated and reconstructed level, it was shown, that the assignment of the jets to the leptons is done better by $krec + jetch$ than by $krec$. A significant improvement in processing speed is shown by the much shorter CPU time per event for $krec + jetch$ (see Sec. 4.2.5).

For future studies on this topic, it would be interesting to look at the effects of using different lepton to jet pairing methods for events with a small separation of the jet charges. Another way of improvement may lay in using a different definition of jet charge than the one described in Sec. 3.2.1, meaning either a different weighing factor k or a different way of determining, whether a track should count as part of the jet.

6 Appendix

6.1 Object definition and event selection

From the Monte Carlo generated data, only events with exactly two leptons with charges of opposite sign and exactly two b -tagged jets were used. The multivariate MV1 b -tagging algorithm is used at a level of 70% b -jet efficiency. The MV1 tagger is based on a neural network which combines several tools and is described in [26]. Both, the leptons and jets, must have a transverse momentum of $p_T > 25$ GeV to be considered. To exclude events with $Z \rightarrow ll$ decays, only events with $|m_{ll} - m_Z| > 10$ GeV were used, where m_{ll} is the combined mass of the two leptons and m_Z the standard model mass of the Z boson. All events must satisfy $H_T > 130$ GeV, where H_T is the sum of the transverse hadronic energy of the two jets and leptons. Furthermore only events were used, where the two leptons are either e or μ . Events with W bosons decaying into τ leptons are included since $\approx 35\%$ of τ leptons almost instantly (inside the beam pipe) decay via $\tau \rightarrow e\bar{\nu}_e\nu_\tau$ or $\tau \rightarrow \mu\bar{\nu}_\mu\nu_\tau$ into e or μ [4]. Those processes would therefore be treated in the same way as processes, in which the W bosons decay directly into e or μ leptons.

6.2 Additional plots

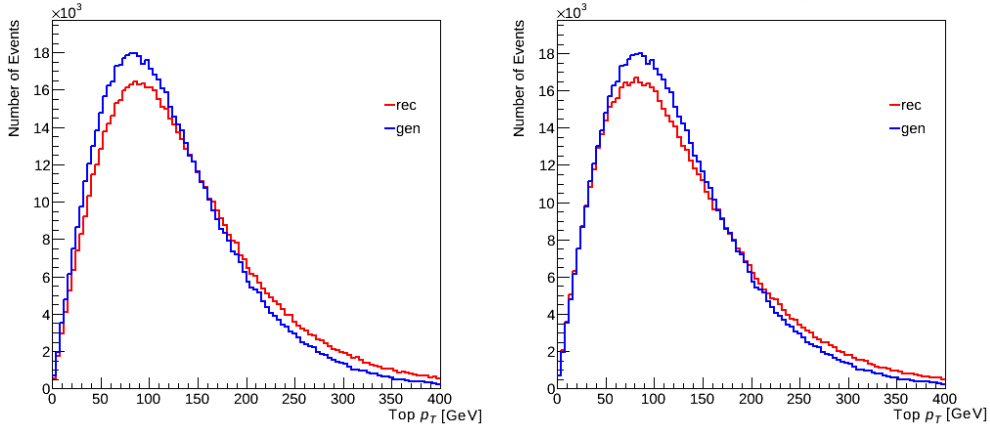


Figure 6.1: Transverse momentum p_T distributions for t at reconstructed (rec) and generated (gen) level for $krec$ [left] and $krec + jetch$ [right].

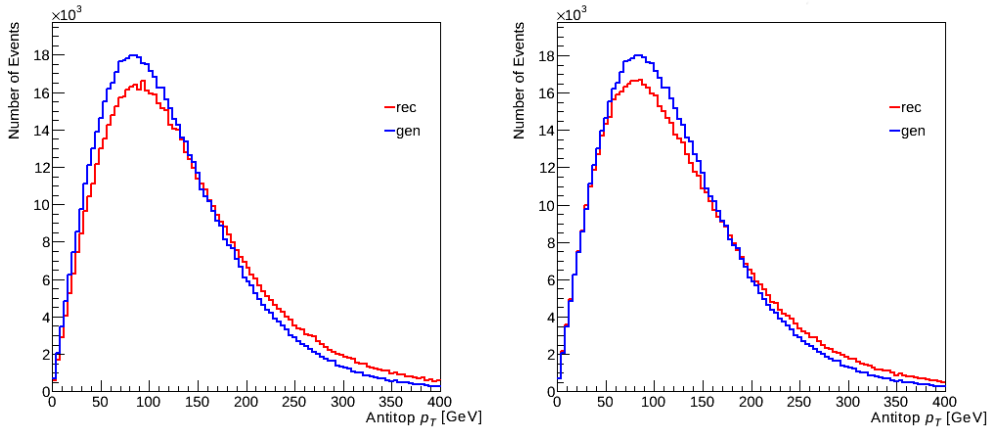


Figure 6.2: Transverse momentum p_T distributions for \bar{t} at reconstructed (rec) and generated (gen) level for $krec$ [left] and $krec + jetch$ [right].

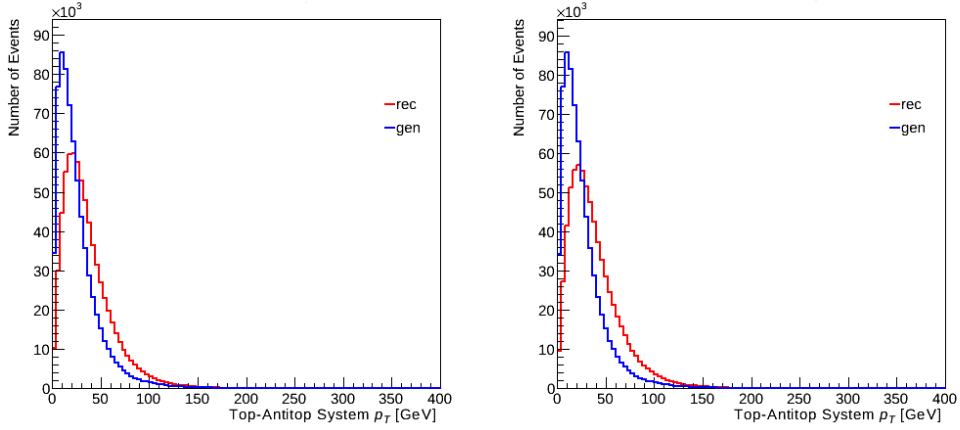


Figure 6.3: Transverse momentum p_T distributions for the $t\bar{t}$ system at reconstructed (rec) and generated (gen) level for $krec$ [left] and $krec + jetch$ [right].

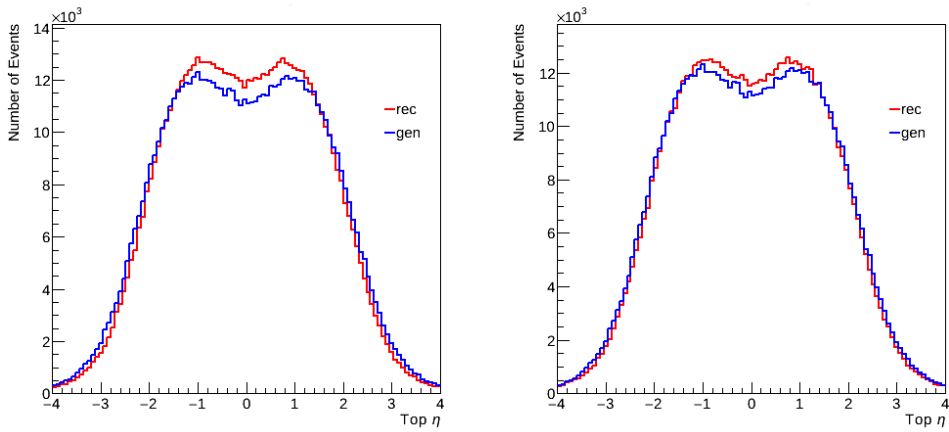


Figure 6.4: Pseudorapidity η distributions for t at reconstructed (rec) and generated (gen) level for $krec$ [left] and $krec + jetch$ [right].

6 Appendix

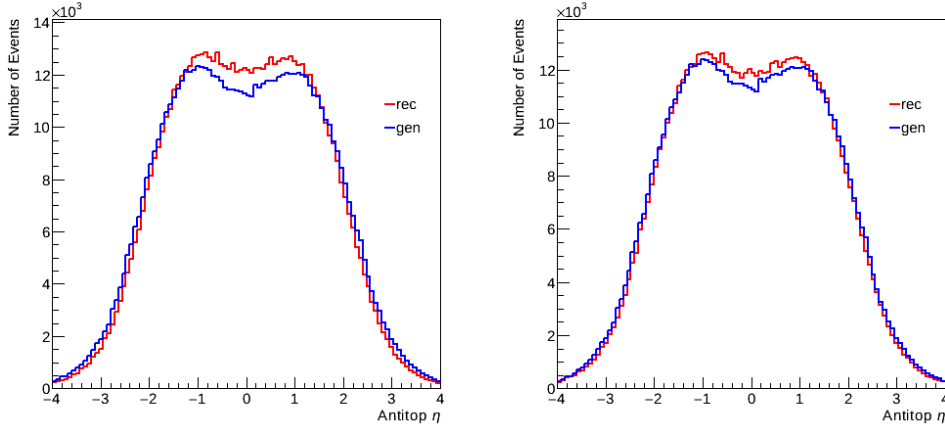


Figure 6.5: Pseudorapidity η distributions for \bar{t} at reconstructed (rec) and generated (gen) level for $krec$ [left] and $krec + jetch$ [right].

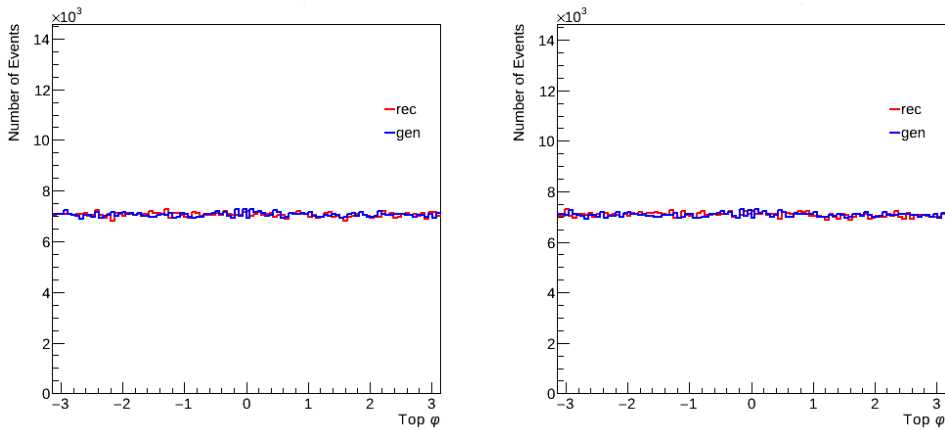


Figure 6.6: Azimuthal angle φ distributions for t at reconstructed (rec) and generated (gen) level for $krec$ [left] and $krec + jetch$ [right].

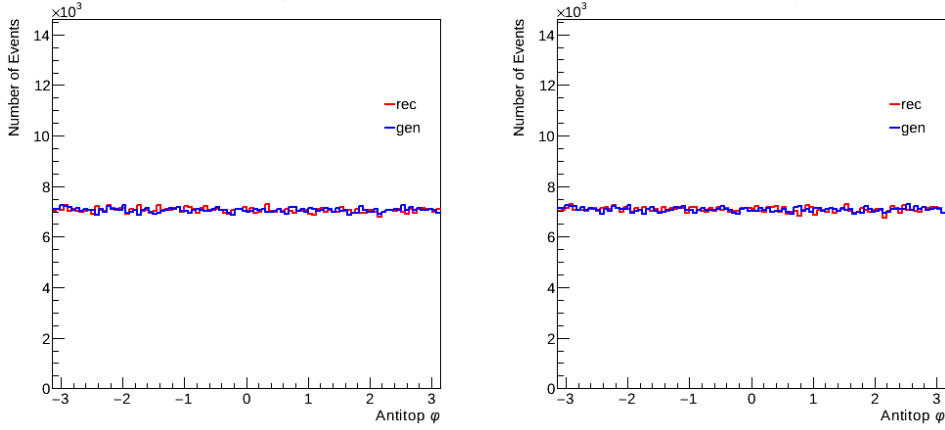


Figure 6.7: Azimuthal angle φ distributions for \bar{t} at reconstructed (rec) and generated (gen) level for $krec$ [left] and $krec + jetch$ [right].

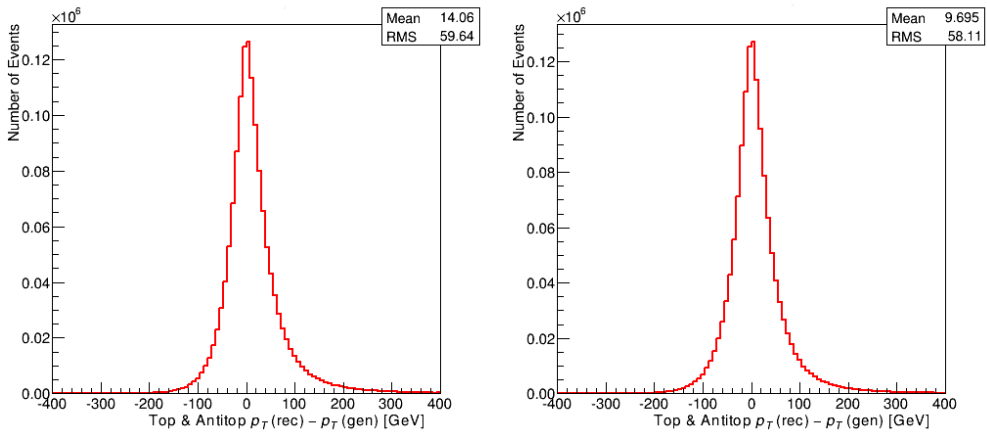


Figure 6.8: Resolution of transverse momentum $p_T(\text{rec}) - p_T(\text{gen})$ for t and \bar{t} filled in the same histograms for $krec$ [left] and $krec + jetch$ [right].

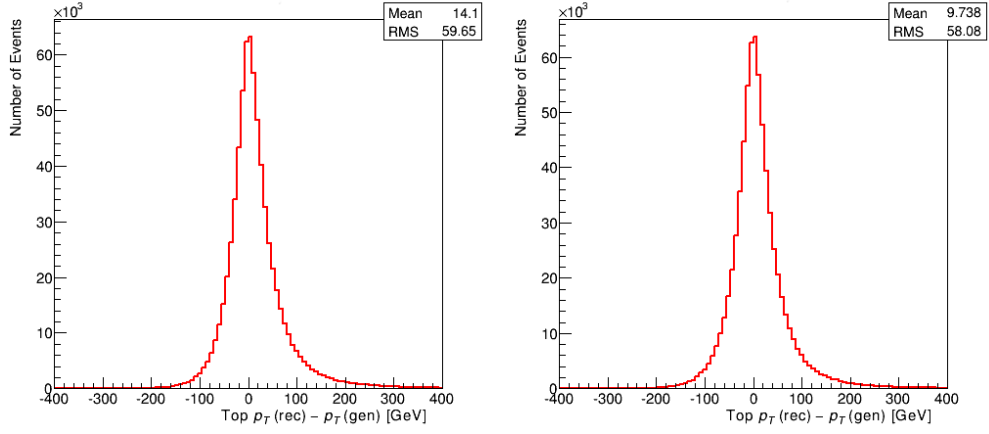


Figure 6.9: Resolution of transverse momentum $p_T(\text{rec}) - p_T(\text{gen})$ for t for k_{rec} [left] and $k_{rec} + j_{etch}$ [right].

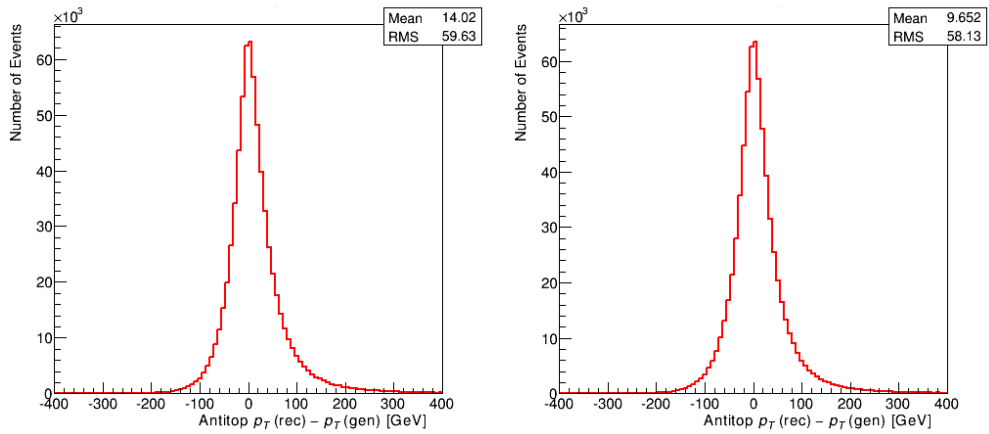


Figure 6.10: Resolution of transverse momentum $p_T(\text{rec}) - p_T(\text{gen})$ for \bar{t} for k_{rec} [left] and $k_{rec} + j_{etch}$ [right].

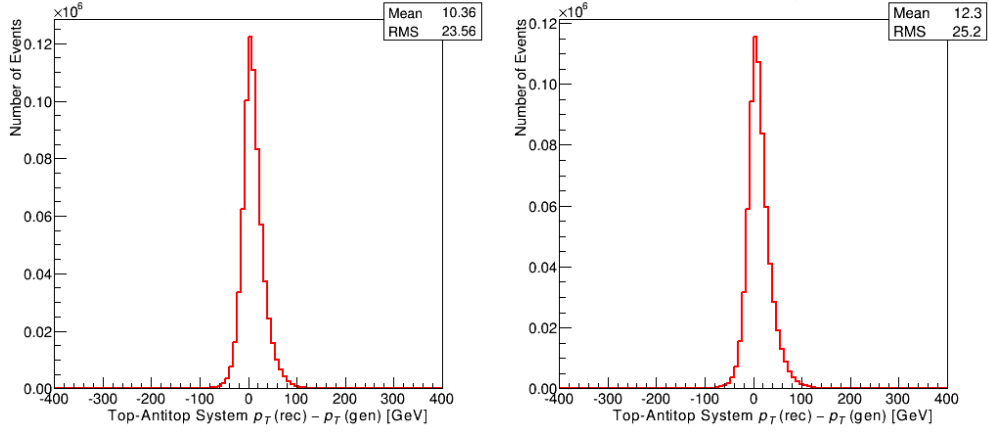


Figure 6.11: Resolution of transverse momentum $p_T(\text{rec}) - p_T(\text{gen})$ for the $t\bar{t}$ system for k_{rec} [left] and $k_{\text{rec}} + j_{\text{etch}}$ [right].

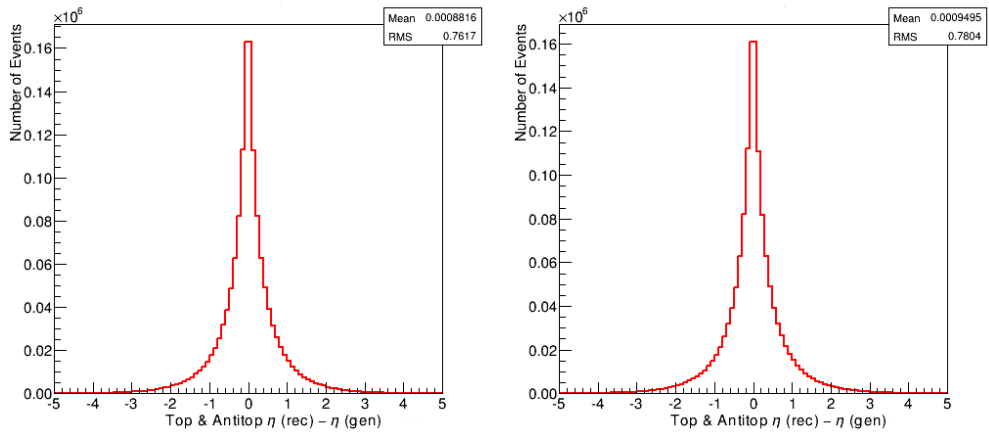


Figure 6.12: Resolution of pseudorapidity $\eta(\text{rec}) - \eta(\text{gen})$ for t and \bar{t} filled in the same histograms for k_{rec} [left] and $k_{\text{rec}} + j_{\text{etch}}$ [right].

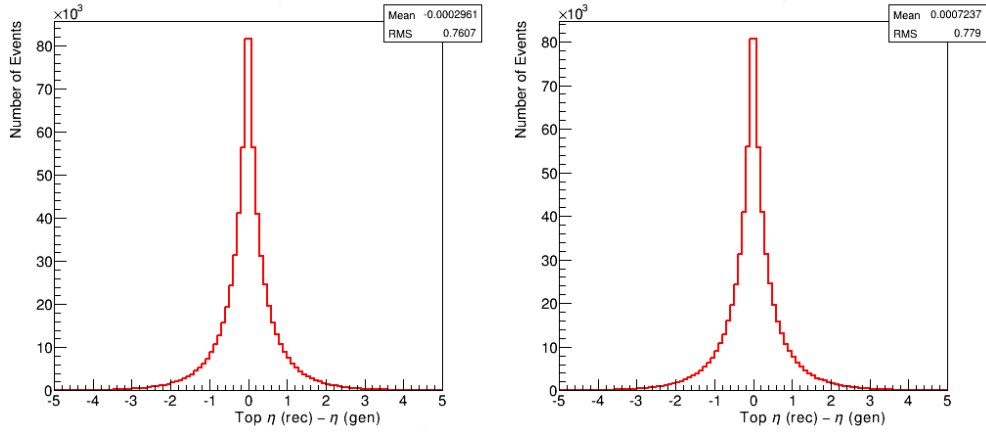


Figure 6.13: Resolution of pseudorapidity $\eta(\text{rec}) - \eta(\text{gen})$ for t for $krec$ [left] and $krec + jetch$ [right].

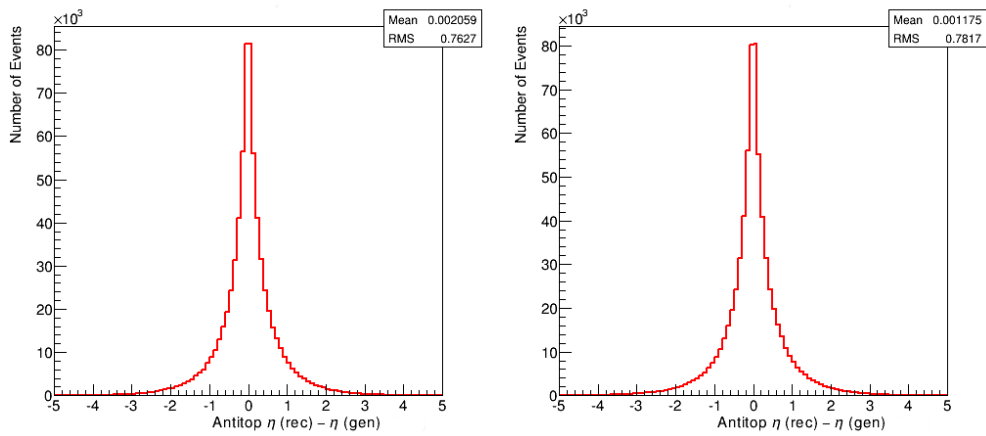


Figure 6.14: Resolution of pseudorapidity $\eta(\text{rec}) - \eta(\text{gen})$ for \bar{t} for $krec$ [left] and $krec + jetch$ [right].

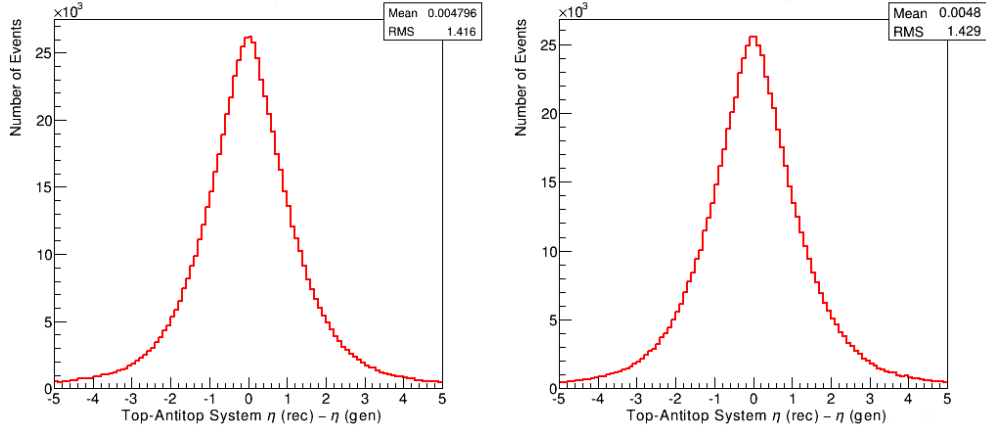


Figure 6.15: Resolution of pseudorapidity $\eta(\text{rec}) - \eta(\text{gen})$ for the $t\bar{t}$ system for $k\text{rec}$ [left] and $k\text{rec} + j\text{etch}$ [right].

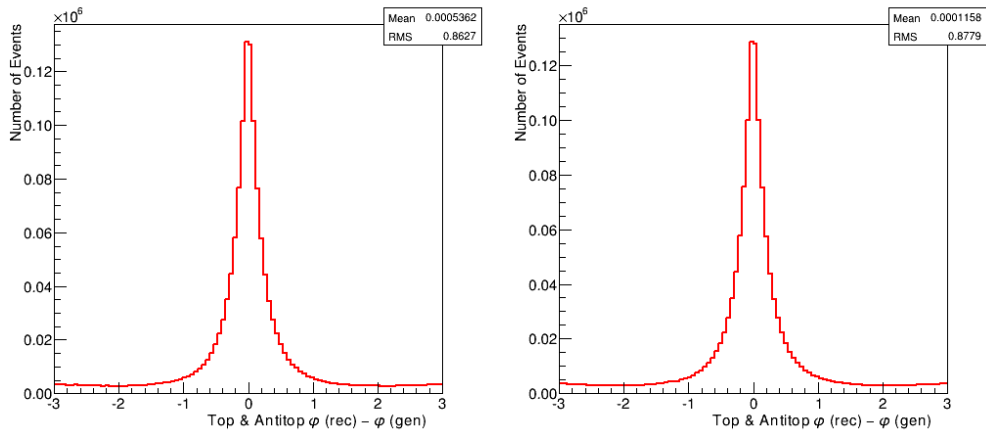


Figure 6.16: Resolution of azimuthal angle $\varphi(\text{rec}) - \varphi(\text{gen})$ for t and \bar{t} filled in the same histograms for $k\text{rec}$ [left] and $k\text{rec} + j\text{etch}$ [right].

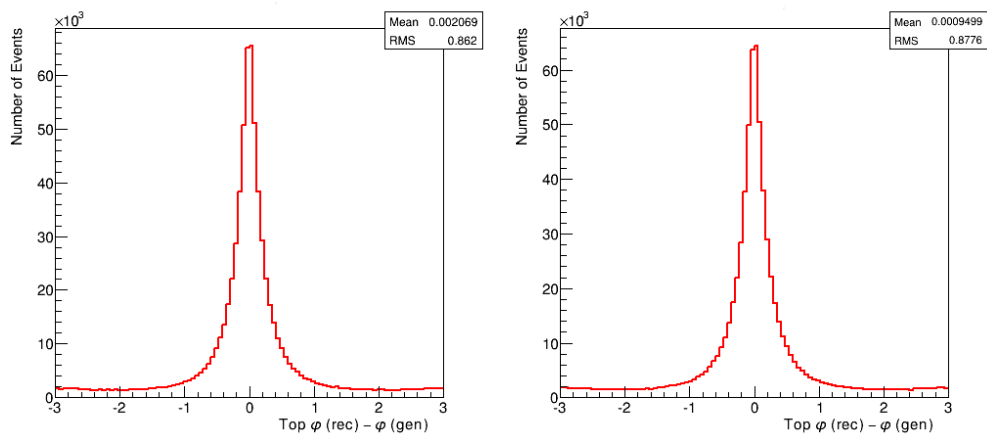


Figure 6.17: Resolution of azimuthal angle $\varphi(\text{rec})-\varphi(\text{gen})$ for t for $k\text{rec}$ [left] and $k\text{rec}+j\text{etch}$ [right].

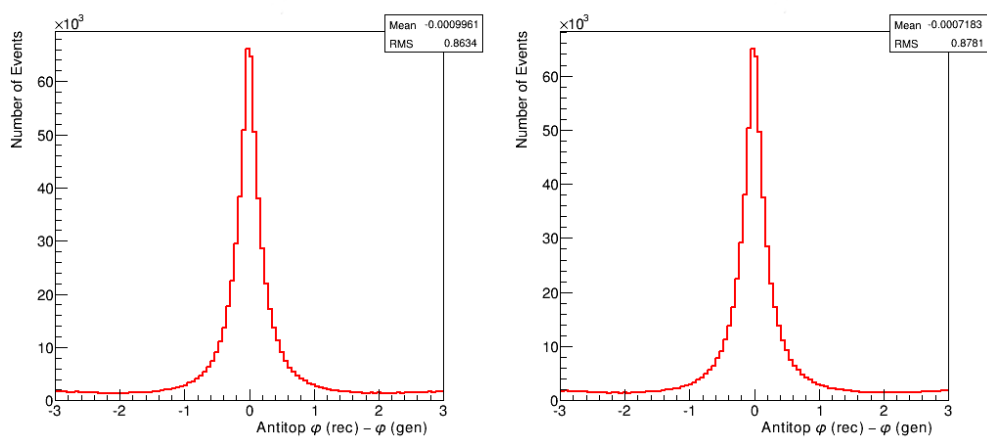


Figure 6.18: Resolution of azimuthal angle $\varphi(\text{rec})-\varphi(\text{gen})$ for \bar{t} for $k\text{rec}$ [left] and $k\text{rec}+j\text{etch}$ [right].

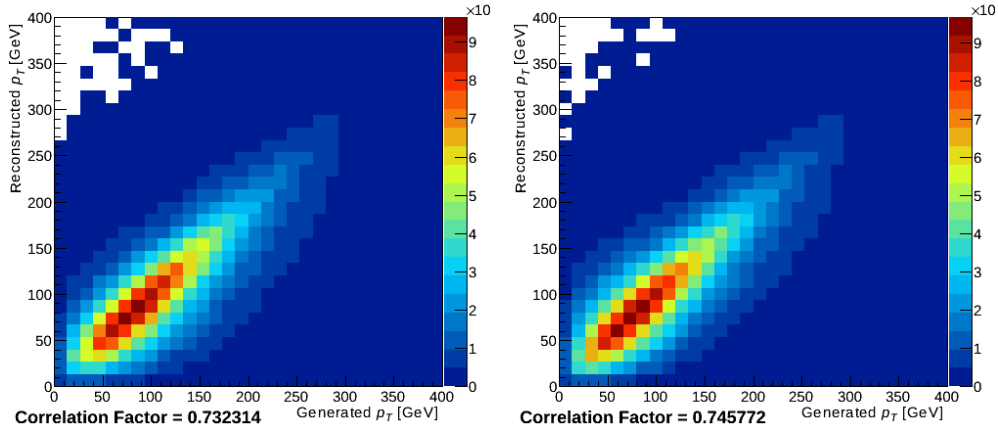


Figure 6.19: Reconstructed over generated transverse momentum p_T for t for *krec* [left] and *krec + jetch* [right].

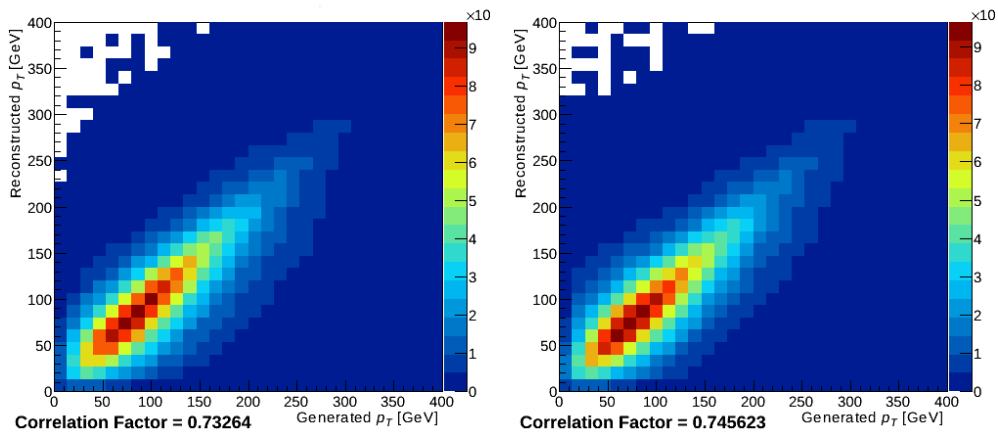


Figure 6.20: Reconstructed over generated transverse momentum p_T for \bar{t} for *krec* [left] and *krec + jetch* [right].

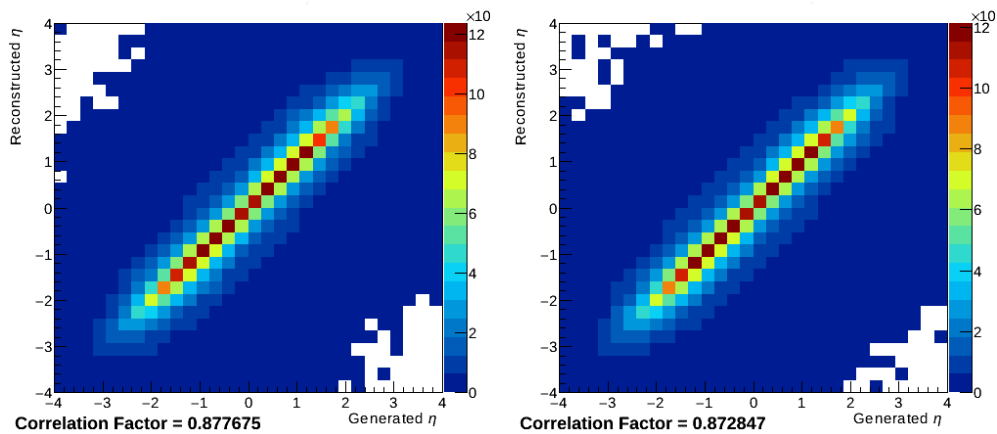


Figure 6.21: Reconstructed over generated pseudorapidity η for t for $krec$ [left] and $krec + jetch$ [right].

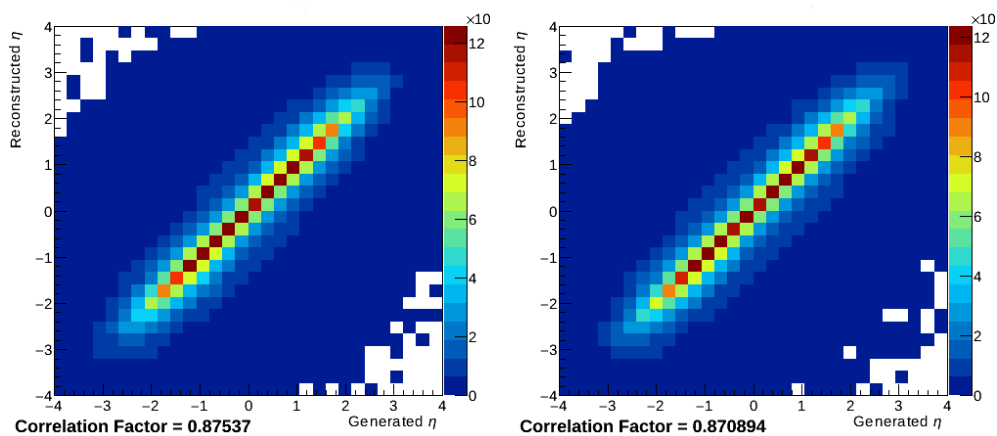


Figure 6.22: Reconstructed over generated pseudorapidity η for \bar{t} for $krec$ [left] and $krec + jetch$ [right].

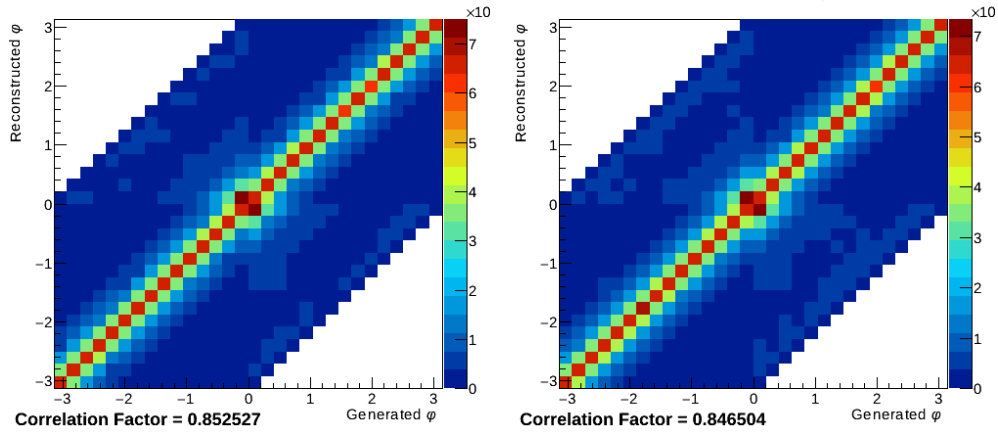


Figure 6.23: Reconstructed over generated azimuthal angle φ for t for k_{rec} [left] and $k_{rec} + j_{etch}$ [right].

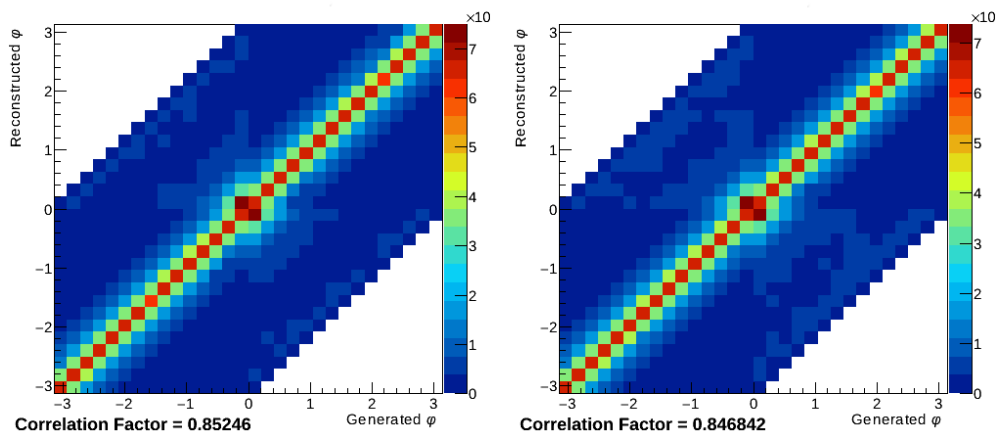


Figure 6.24: Reconstructed over generated azimuthal angle φ for \bar{t} for k_{rec} [left] and $k_{rec} + j_{etch}$ [right].

6 Appendix

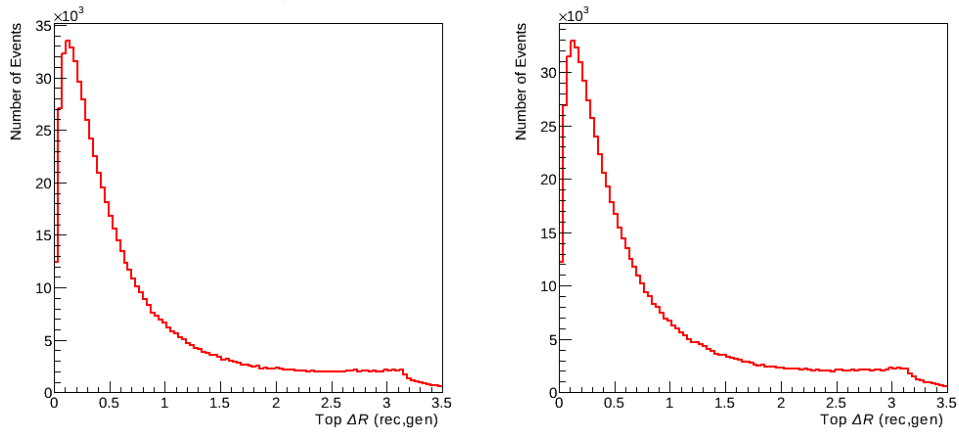


Figure 6.25: $\Delta R := \sqrt{\Delta\varphi^2 + \Delta\eta^2}$ between reconstructed and generated t for *krec* [left] and *krec + jetch* [right].

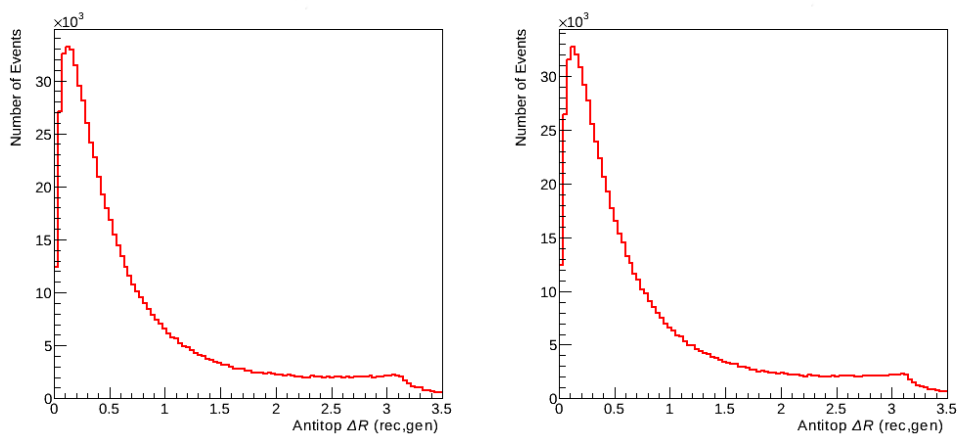


Figure 6.26: $\Delta R := \sqrt{\Delta\varphi^2 + \Delta\eta^2}$ between reconstructed and generated \bar{t} for *krec* [left] and *krec + jetch* [right].

Bibliography

- [1] ATLAS, CDF, CMS and DØ collaboration, *First combination of Tevatron and LHC measurements of the top-quark mass* (2014), 1403.4427
- [2] J. Gao, C. S. Li, H. X. Zhu, *Top Quark Decay at Next-to-Next-to Leading Order in QCD*, Phys.Rev.Lett. **110**(4), 042001 (2013)
- [3] T. A. Aaltonen, et al. (CDF), *Direct Measurement of the Total Decay Width of the Top Quark*, Phys.Rev.Lett. **111**(20), 202001 (2013)
- [4] K. Olive, et al. (Particle Data Group), *Review of Particle Physics*, Chin.Phys. **C38**, 090001 (2014)
- [5] I. I. Bigi, et al., *Production and Decay Properties of Ultraheavy Quarks*, Phys.Lett. **B181**, 157 (1986)
- [6] A. Quadt, *Top quark physics at hadron colliders*, Eur.Phys.J. **C48**, 835 (2006)
- [7] J. Christenson, et al., *Evidence for the 2π Decay of the $k(2)0$ Meson*, Phys.Rev.Lett. **13**, 138 (1964)
- [8] M. Kobayashi, T. Maskawa, *CP Violation in the Renormalizable Theory of Weak Interaction*, Prog.Theor.Phys. **49**, 652 (1973)
- [9] M. L. Perl, et al., *Evidence for Anomalous Lepton Production in $e^+ - e^-$ Annihilation*, Phys.Rev.Lett. **35**, 1489 (1975)
- [10] S. Herb, et al., *Observation of a Dimuon Resonance at 9.5-GeV in 400-GeV Proton-Nucleus Collisions*, Phys.Rev.Lett. **39**, 252 (1977)
- [11] S. Abachi, et al. (D0), *Search for high mass top quark production in $p\bar{p}$ collisions at $\sqrt{s} = 1.8$ TeV*, Phys.Rev.Lett. **74**, 2422 (1995)
- [12] F. Abe, et al. (CDF), *Observation of top quark production in $\bar{p}p$ collisions*, Phys.Rev.Lett. **74**, 2626 (1995)

Bibliography

- [13] O. S. Bruning, et al., *LHC Design Report Vol.1: The LHC Main Ring* (2004)
- [14] J. Arpad Horvath, *LHC 02* (2012), URL http://de.wikipedia.org/wiki/Datei:LHC_02.svg
- [15] S. Artz, et al., *Upgrade of the ATLAS Central Trigger for LHC Run-2*, JINST **10(02)**, C02030 (2015)
- [16] P. S. Joao Pequena0 (CERN), *How ATLAS works* (2013), URL <http://www.atlas.ch/photos/full-detector.html>
- [17] J. Pequena0 (CERN), *Computer generated image of the whole ATLAS detector* (2008), URL <http://www.atlas.ch/photos/full-detector-cgi.html>
- [18] G. Aad, et al. (ATLAS), *Operation and performance of the ATLAS semiconductor tracker*, JINST **9**, P08009 (2014)
- [19] G. Aad, et al. (ATLAS), *Observation of a new particle in the search for the Standard Model Higgs boson with the ATLAS detector at the LHC*, Phys.Lett. **B716**, 1 (2012)
- [20] S. Chatrchyan, et al. (CMS), *Observation of a new boson at a mass of 125 GeV with the CMS experiment at the LHC*, Phys.Lett. **B716**, 30 (2012)
- [21] ATLAS collaboration, *Combination of searches for strongly-produced supersymmetric particles with the ATLAS detector in proton-proton collision data at $\sqrt{s}=8$ TeV*, ATLAS-CONF-2015-011 (2015)
- [22] *Performance studies of $t\bar{t}$ reconstruction methods in the dilepton channel at $\sqrt{s} = 8$ TeV in ATLAS*, ATL-COM-PHYS-2014-226 (2014)
- [23] G. Aad, et al. (ATLAS), *Measurement of the top quark charge in pp collisions at $\sqrt{s} = 7$ TeV with the ATLAS detector*, JHEP **1311**, 031 (2013), 1307.4568
- [24] R. D. Field, R. P. Feynman, *A Parametrization of the Properties of Quark Jets*, Nucl. Phys. **B136**, 1 (1978)
- [25] J. Erdmann, et al., *A likelihood-based reconstruction algorithm for top-quark pairs and the KLFitter framework*, Nucl. Instrum. Meth. **A748**, 18 (2014)
- [26] *Commissioning of the ATLAS high-performance b-tagging algorithms in the 7 TeV collision data*, ATLAS-CONF-2011-102 (2011)

Acknowledgements

In first instance, I want to thank Prof. Dr. Arnulf Quadt not only for providing me with the chance to write my bachelor's thesis in the subject of particle physics, but also for his enthusiastic way of explaining the fundamentals needed for the thesis in the Spezialisierungspraktikum before the beginning of the work on my thesis. I also want to thank Prof. Dr. Ariane Frey for agreeing to be the second referee and for her vivid way of presenting the basic principles of particle physics in her lectures, which were one reason, why I chose to write my thesis in this topic.

Special thanks go out to Dr. Boris Lemmer and Gvantsa Mchedlidze for supporting me in the process of writing the thesis, for providing me with material on the topic and for proof reading. I am very thankful to them for answering all my questions. Without their extensive help, it would not have been possible for me to finish the thesis.

Erklärung

nach §13(9) der Prüfungsordnung für den Bachelor-Studiengang Physik und den Master-Studiengang Physik an der Universität Göttingen:

Hiermit erkläre ich, dass ich diese Abschlussarbeit selbständig verfasst habe, keine anderen als die angegebenen Quellen und Hilfsmittel benutzt habe und alle Stellen, die wörtlich oder sinngemäß aus veröffentlichten Schriften entnommen wurden, als solche kenntlich gemacht habe.

Darüberhinaus erkläre ich, dass diese Abschlussarbeit nicht, auch nicht auszugsweise, im Rahmen einer nichtbestandenenen Prüfung an dieser oder einer anderen Hochschule eingereicht wurde.

Göttingen, den 13. März 2016

(Tobias Fitschen)